POLITECNICO DI TORINO

Master's Degree in Automotive Engineering

Politecnico
di Torino

Manufacturing of complex geometries by means of DED-LB technology

Supervisors

Prof. Eleonora ATZENI

Prof. Alessandro SALMI

Ing. Adriano PILAGATTI

Candidate

Paolo RUSSO

NOVEMBER 2025

Summary

This thesis investigates the realization of complex metallic geometries through Laser Directed Energy Deposition (DED-LB) technology, with the aim of assessing the feasibility and limitations of the process when applied to challenging shapes. The study focuses on two representative case studies characterized by unsupported overhangs, inclined surfaces, and the requirement of continuous deposition.
The methodology involves defining planar slicing planes based on the geometric features of the components, in order to reproduce the sectional layers used for the deposition process. The slicing was performed using Rhinoceros Grasshopper, which was employed to extract the necessary point coordinates from the CAD model. Subsequently, a MATLAB script was developed to generate the corresponding G-code, customized according to the capabilities of the Prima Additive LASERDYNE 430® system and designed to control layer alternation, pauses, and retraction routines.
Experimental trials were conducted to evaluate both the geometrical accuracy and the overall quality of the manufactured parts. The results confirm the feasibility of producing complex tubular junctions through L-DED, while highlighting critical aspects such as material accumulation, thermal management, and dimensional accuracy, particularly in curved or inclined regions.
Overall, the work demonstrates that, with a suitable planar slicing strategy and dedicated G-code generation, L-DED technology can effectively manufacture geometrically complex parts, providing a reproducible framework for the automation of toolpath generation and the optimization of deposition parameters.

Acknowledgements

A Mamma, Papà e Dado, le cose possono anche non funzionare bene, ma l'impegno per ripararle è ciò che è sempre contato.

Agli amici di Palermo: Ciccio, Atomik, Riccardo S., Ettore, Valerio, Andrea, Gabriele, Sofia, Marta, Giulia, Ignazio e Riccardo C. . Vi voglio bene oramai da anni. Sono cresciuto grazie a voi e con voi, e chi sono oggi è anche merito vostro.

Ai colleghi di Torino: Edoardo, Riccardo, Andrea e Jabrooth. Siete gli ingegneri migliori che io conosca, ma soprattutto degli amici fantastici. Non sarei sopravvissuto al Politecnico senza di voi.

A Sambuca, che mi ha permesso di non perdere me stesso.

A chi oggi è presente e a chi non può esserci, col petto pieno di orgoglio posso dire di avercela fatta nella vita, e non per questo inutile pezzo di carta, ma perchè fate parte della mia vita anche quando è difficile starmi accanto.
Non sono mai stato solo, ma solo in un posto diverso dal vostro.

Grazie.

"Non quia difficilia sunt non audemus, sed quia non audemus difficilia sunt."
— Seneca

Table of Contents

List of Tables

List of Figures

Acronyms

AI
artificial intelligence

AM
Additive Manufacturing

DfAM
Design for Additive Manufacturing

DED
Directed Energy Deposition

DED-LB
Laser Directed Energy Deposition

LP-DED
Laser Powder Directed Energy Deposition

PBF
Powder Bed Fusion

MRO
Mainenance, Repair and Overhaul activities

KPVs
Key Performance Variable(s)

PSC
Part Surface Coordinates

Chapter 1

Introduction

1.1 Additive Manufacturing

1.1.1 Background

Additive manufacturing (AM) is a manufacturing process already introduced in the '80s and better known as *3D printing*, that consists in creating an object adding layer by layer the material starting from a digital model. The application fields are many such as Aerospace, Automotive and Medical, and it can be exploited with different materials like metals, polymers, ceramics, and many more. This is due to the fact that AM is characterized by many advantages such as reduced complexity of the supply chain, rapid prototyping, the ability to realize complex geometries that traditional processes cannot.
Different technologies can be used depending on the family of the material and the shape it comes in according to the **ISO-ASTM 52900-21** [1]

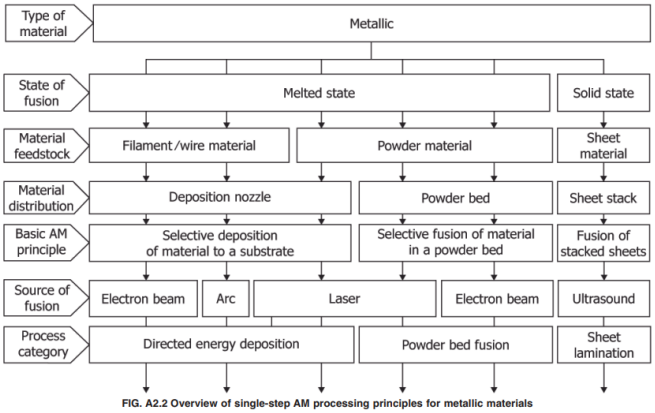

Figure 1.1: Overview of single-step AM processing principles for metallic materials [1]

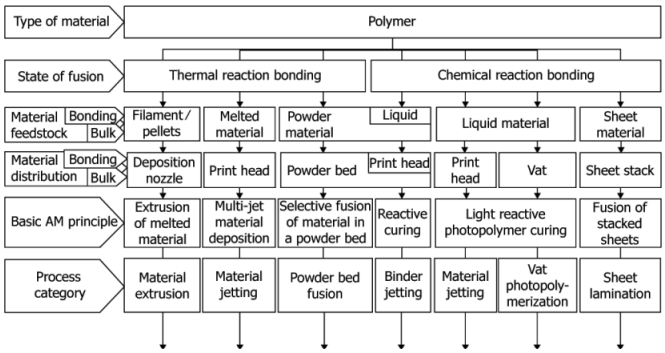

Figure 1.2: Overview of single-step AM processing principles for polymer materials [1]

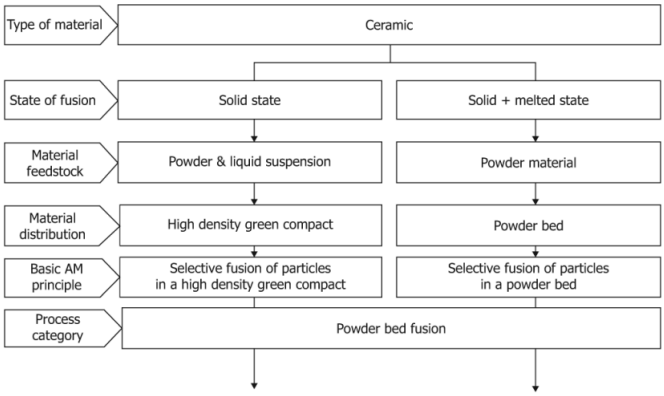

Figure 1.3: Overview of single-step AM processing principles for ceramic materials [1]

The growing relevance that AM is conquering among different industrial fields is due to its intrisical advantages such as:

- The chance to realize extremely complex geometries - such as lattice structures, internal channels, or lightweight topologically optimized parts — wich are usually difficult to realize through traditional processes. [2];
- a simpler and more flexible supply chain, characterized by a reduction of the required tools and the chance of *on-demand* and distributed production. [3];
- fast prototyping and delivery time reduction thanks to process digitalization and direct integration between design and fabrication [4];
- wide range of materials avaliable — polymers, ceramiccs, metals and composites — that widens the application field of the technology [5].

Thanks to these characteristics, AM represents a key enabling technology in sectors such as aerospace, automotive, and biomedical engineering. For example, in the aerospace sector lightweight composites are adopted for structural components, turbine parts, and cooling channels integrated within complex geometries [6]. In the Automotive sector, the research is focused on the *Design for Additive Manufacturing* (DfAM), Nel settore automotive, la ricerca si concentra sul *Design for Additive Manufacturing* (DfAM), with the purpose of realizing lighter, functonally integrated and customized components.[7].
Nevertheless, several challenges still limit the full industrial maturity of AM: process qualification, repeatability, standardization, traceability, post-processing requirements, and surface quality control remain active areas of research [8].
In this context this thesis proposes to investigate the realizations of complex geometries by means of *Laser-Directed Energy Deposition* (DED-LB), in particular

the realization of a T-Shaped tube and a Spiral Junction of multiple tubes.
The purpose is to analyze the feasibility of the geometries together with all the workflow—from digital modeling to process execution—including G-code generation, layer-wise toolpath design, and experimental validation.
If we want to classify the AM processes suitable for the manufacturing of metals we can find three layers of characterization:

1. Category
2. Feedstock
3. Process

1.1.2 Directed energy deposition

Since the geometries studied in this thesis are thin-wall tubes, the selected technology is Directed Energy Deposition (DED). In a DED, three are the main featues that chracterize a machine:

- The thermal source
  That can be an Electron Beam, a Laser or an Electric Arc
- The feedstock
  That can be powder (as in this case) or wire
- The protective gas

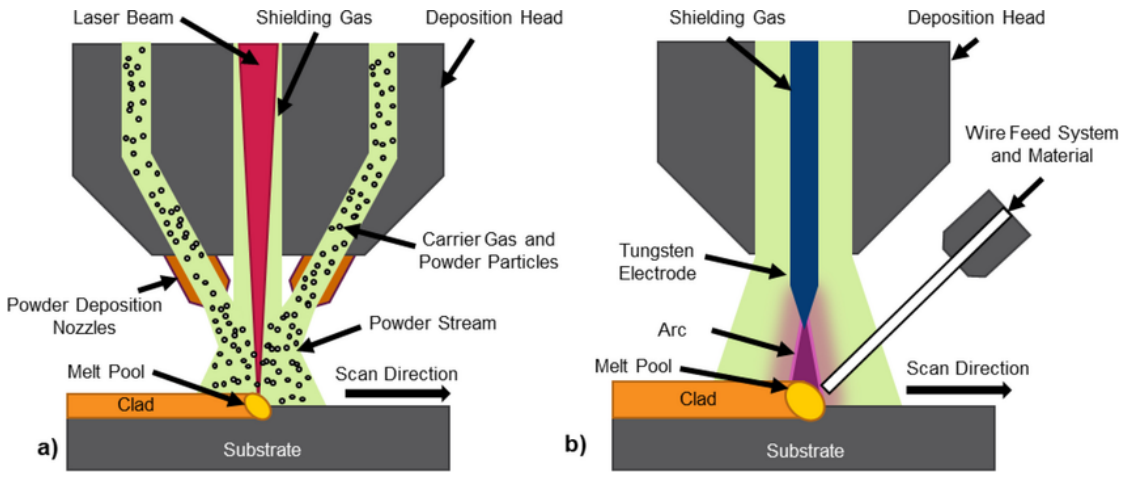

Figure 1.4: left:Powder-based DED - right:Wire-based DED

Wire DED

Wire-based Directed Energy Deposition (W-DED)(Fig:1.4) is an AM process that exploits a metallic wire as the addition material. The wire is fed directly into the

melt pool generated by a focused thermal source, typically a high-power laser or an electron beam, and is protected by an inhert gas.
It is primarily utilized for MRO activities but also for the realization of new objects. Some examples of applications of W-DED come from NASA in Figure 1.5

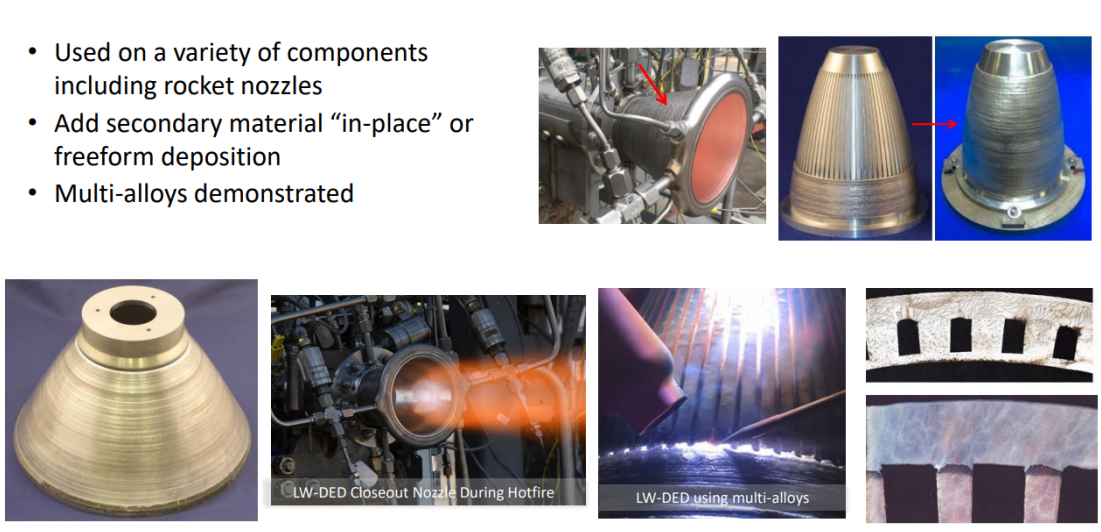

Figure 1.5: Screenshot taken from the presentation titled *"Principles of Directed Energy Deposition for Aerospace Applications"*, Slide 25

If we want to address the pros and the cons of the technology:

Pros

- **High material usage efficiency**: The wire is used almost at 100%
- **Cheaper feedstock**: The wire is cheaper than fine powder
- **Less safety issues**: The wire is not flammable or dangerous if inhaled

Cons

- **Very low resolution**: The resolution is limited by the thickness of the wire
- **High porosity**: The final parts might present internal defects or cavities if the KPVs are not controlled
- **Less materials avaliable**:The wire feedstocks present a limited variety of metals

Powder DED

This technology consists in feeding the powder which is transported directly by the inert gas (as seen in Fig1.4) and simultaneously melted by the thermal source. Thanks to its higer resolution compared to the Wire DED, it results to be more suitable for geometries that require an higher level of resolution. It can be used for MRO applications as well, but also for large scale manufacturing that present small features as seen in Fig 1.6

Figure 1.6: Large scale manufacturing examples from *"Principles of Directed Energy Deposition for Aerospace Applications" by NASA*, Slide 21

Pros

- **Higher precision**: The powder feedstock increase the range of minumum resolution that can be achieved
- **Wider availiability of materials**: A larger number of materials come in powder form
- **Better control on the layer**: The powder feedrate helps to better control the layer geometry

Cons

- **Higher cost**: The cost of the material itself and the lower usage efficiency
- **Higer safety concerns**: The powder is flammable and toxic
- **Higher complexity**: The powder feeder is much more complex and expensive

Deposition head

At this point it is very clear that the deposition head is really important as all the thermal source optics, powder feed and shielding gas nozzles, and eventual sensors are all embedded in it. The nozzles' configuration in particular is really important as *"during the deposition process with this configuration*(lateral configuration Figure1.7(a))*the geometry and the characteristics of deposited tracks are direction dependent. To overcome this limitation, the coaxial configuration was introduced. Two types of coaxial deposition heads have been developed. The first uses a discrete number of symmetrically positioned nozzles (Figure1.7(b)), while the second uses a conical nozzle (Figure1.7(c)).* as written in [9]

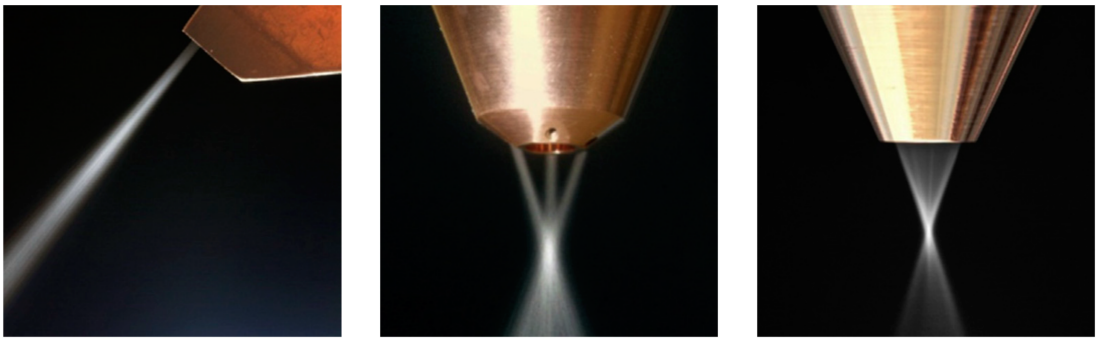

(a) (b) (c)

Figure 1.7: Deposition head configurations: (a) lateral configuration, (b) discrete coaxial configuration, and (c) continuous coaxial configuration

1.1.3 LP-DED KPVs

Overview of the process

In article [9] *"The main mechanisms of the LP-DED process, which are identified as (i) laser irradiation and material addition, (ii) melt pool generation, and (iii) subsequent solidification, are discussed in terms of input parameters, with a focus on their effects on the deposition effectiveness, and interrelation among the mechanisms of the deposition process."*.

Laser irradiation and material addition

The most used nozzle configuration is the coaxial one, but it also causes the powder to be distributed to "focus" in a certain point depending on the taper of the nozzle, as can be seen in Figure 1.8.

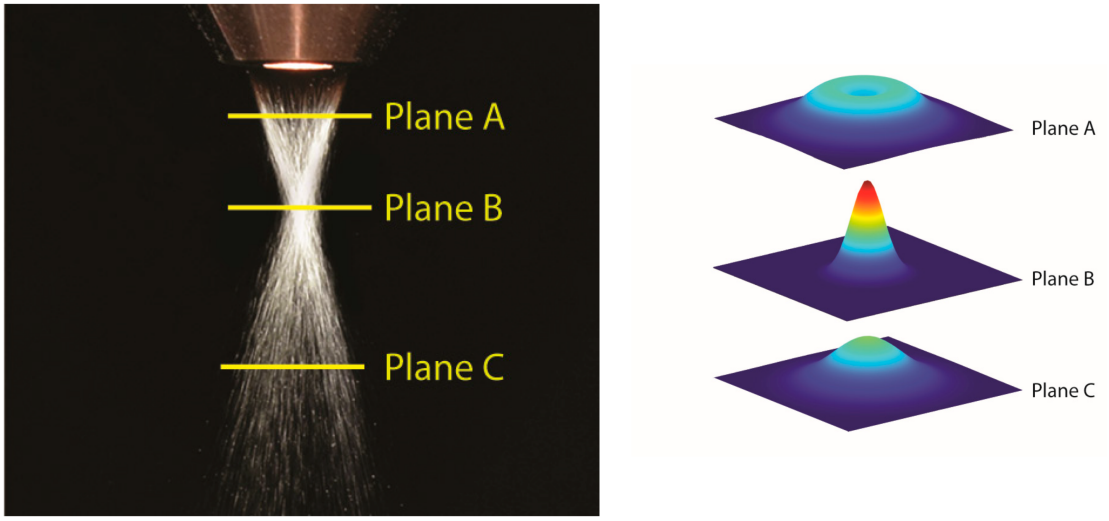

(**a**) (**b**)

Figure 1.8: (a) Experimental and (b) numerical powder distribution evaluated at different planes below the nozzle exit [9]

The actual powder distribution during a print is anyway different as the flow interacts with the previous layer and the walls of the nozzle, but studying the focal point of the stream is important as the powder capture coefficient is maximized because its position determines the point of highest powder mass concentration.
Table 1.1 summarizes the main process parameters that influence the behavior of the powder stream in Powder based DED-LB. Each variable affects specific aspects such as the spatial distribution of the powder, the attenuation of laser power, and the temperature of the particles, ultimately impacting the efficiency and quality of the deposition process.

Process Parameter (KPV)	**Powder Flow Distribution and Velocity at the Substrate**	**Laser Power Attenuation**	**Powder Temperature**
Deposition head design	Influences the powder distribution and velocity	Modifies the shape of the powder stream	-
Stand-off distance	Changes the spatial distribution	Influences velocity and direction	Shifts the plane of maximum concentration
Powder morphology	-	-	Influences thermal absorption
Powder feed rate	-	Influences concentration and attenuation	Increases the temperature of the particles
Material properties	-	Influences the localization of the powder cloud	Determines thermal absorption
Gas flow	-	Modifies the trajectory of the powder stream	Modifies the plane of concentration
Laser power	-	-	Directly heats the particles

Table 1.1: Summary of the factors influencing laser irradiation and material addition mechanisms.

Melt pool generation

Table 1.2 provides an overview of how key process variables affect the temperature distribution, melt pool dimensions, and melt pool morphology during Powder DED-LB. Understanding these relationships is crucial for controlling the melting process and achieving the desired part properties.

Process Parameter (KPV)	**Temperature Distribution**	**Melt Pool Dimension**	**Melt Pool Morphology**
Laser power attenuated	Influences the distribution and the peak of temperature in the melt pool	Determines the height, width, and penetration depth	-
Travel speed	-	Determines the height, width, and penetration depth	-
Powder flow distribution and velocity	-	Determines the height, width, and penetration depth	-
Material properties	-	Determines the height, width, and penetration depth	Determines the shape of the melt pool
Marangoni flows and buoyancy forces	-	-	Determines the shape of the melt pool

Table 1.2: Summary of the factors influencing the melt pool generation mechanisms.

Solidification mechanisms

Table 1.3 illustrates the effects of the main process parameters on the resulting microstructure, residual stress, and surface quality of LP-DED fabricated parts. The careful selection and control of these variables are essential to optimize mechanical performance and surface finish.

Process Parameter (KPV)	**Microstructure**	**Residual Stress**	**Surface Quality**
Material properties	Controls the morphology and dimension of grains	Influences the internal stress state and part/substrate distortions	-
Thermal gradient and solidification rate	Controls the morphology and dimension of grains	Influences the internal stress state and part/substrate distortions	-
Laser power	Controls the morphology and dimension of grains	Influences the internal stress state and part/substrate distortions	Influences the surface roughness and dimensional accuracy
Travel speed	Controls the morphology and dimension of grains	Influences the internal stress state and part/substrate distortions	Influences the surface roughness and dimensional accuracy
Powder flow rate	Controls the morphology and dimension of grains	-	Influences the surface roughness and dimensional accuracy
Deposition strategy	Controls the morphology and dimension of grains	Influences the internal stress state and part/substrate distortions	Influences the surface roughness and dimensional accuracy
Substrate temperature	-	Influences the internal stress state and part/substrate distortions	-

Table 1.3: Summary of the factors influencing the solidification mechanisms.

1.2 LASERDYNE 430 - The machine

1.2.1 General Overview

The machine that was used to conduct the experiments is the **LASERDYNE 430®** from *Prima Additive*, in particular the 5-axis version equipped with the DED-LB head. The machine management happens through the control panel **System 94P** while the feedstock control is enabled by the *powder feeder*.
It is capable to reach a printing rate of 40-50 cm3/h while maintaining a good accuracy and resolution of the print.

1.2.2 Main technical specification

The printing chamber

As mentioned before the machine works with 5-axis, three are linear (**X,Y,Z**) and create a *Cartesian triad* and two are rotational (**A and B**) and allow a rotation about the . The **Z-axis** is the "vertical" one and is assigned to the tool head, while **X** (the longest axis) and **Y** movements, and **A** and **B** rotations are assigned to the deposition plate. A better understanding of the set-up can be achieved by looking at Figure 1.9.

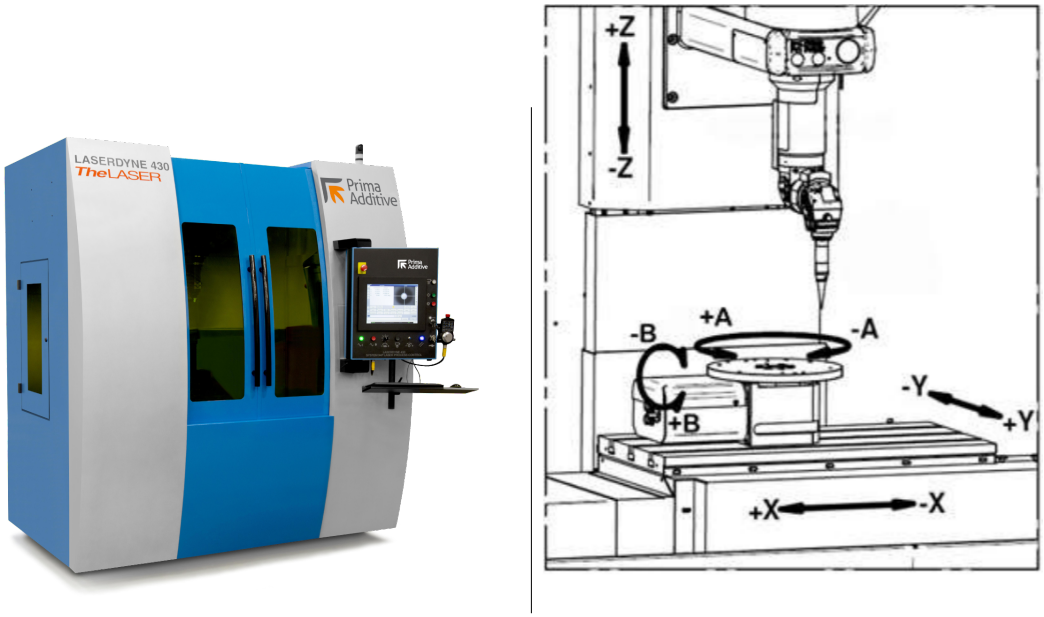

(a) a) **(b)** b)

Figure 1.9: a) LASERDYNE 430®b) Axis configuration [10]

The entity of the achievable displacements, and therefore the achievable printing volume, for each axis is reported in Table 1.4.

Axis	Displacement/Rotation
X	585 mm
Y	408 mm
Z	508 mm
B	+60 / -240°
A	∞

Table 1.4: Axis specifications

Deposition head

The Deposition head (Figure 1.10) is equipped with a coaxial nozzle and is quipped with a fiber laser as thermal source. In Table 1.5 are gathered some of the main aspects of the head from [10].

Figure 1.10: Deposition head

Aspect	Detail
Laser Power	1-kW (fiber laser, CW or QCW)
Spot Size	Approximately 0.3–1 mm diameter
Focal Distance	8 mm
Powder Feeding	Coaxial Nozzle
Shielding Gas	Argon, nitrogen, or other inert gases
Cooling	Air cooling system
Sensors	Temperature and melt pool monitoring

Table 1.5: Key features of the LASERDYNE 430 L-DED deposition head

Control Panel System 94P

Figure 1.11: Control Panel System 94P

1.2.3 Present work application

As announced this master thesis will talk about the design and manufacturing of two manufacts. The first one is the pursuance of the Job 1 concluded in [11]. The spiralized tubes need to be joined in one single tube, and the manufact 1 concerns the joint of the three tubes. The second Manufact will instead be a speculation on how to join two perpendicular tubes that form a T-junction. The geometries and approaches are better explained in the chapter **??**.
The preliminar combinations of Feedrate and laser Power are chosen from [12] Figure 1.12 as the material used for the deposition is again **AISI 316L**

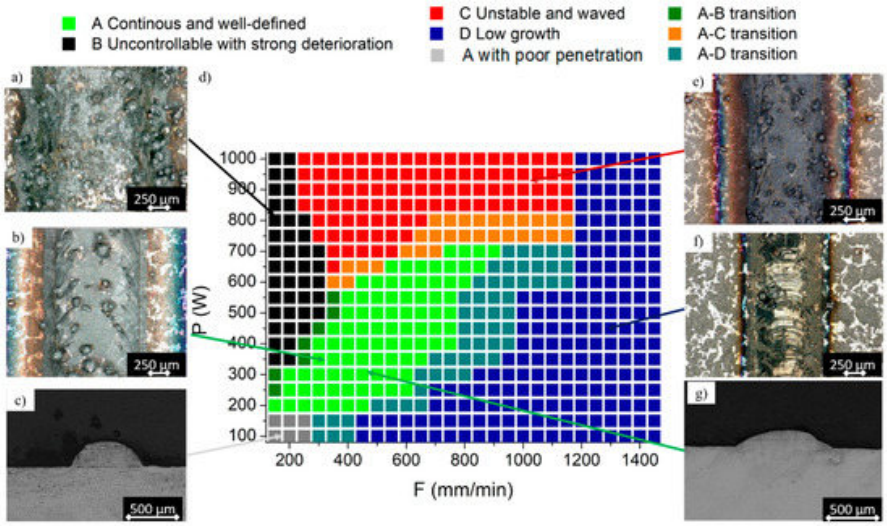

Figure 1.12: AISI 316L process parameter window through single tracks classification.[12]

Chapter 2

The manufacts

2.1 Starting Geometries

As said before, the Geometries that were studied are some sections of the redesign of an actuator from *Cadence Aerospace*. In Figure 2.1 we can see the original part, while in Figure 2.2 we see the whole redesign of the part in [11].

Figure 2.1: Actuator housing from *Cadence Aerospace*

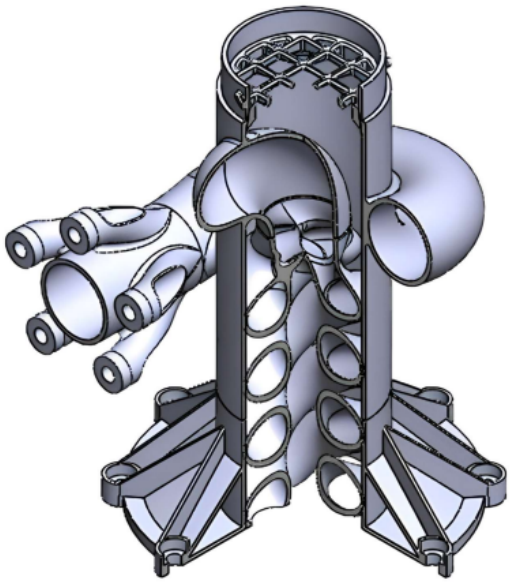

Figure 2.2: Redesigned actuator

Since the the thesis [11] resulted in the successfull realization of the sections in Figure 2.3 and Figure 2.4 but lacked in the completion of the redisgned part, this

thesis proposes some solutions for sections consecutive to the realized ones shown in Figure 2.5 and Figure 2.6.

Figure 2.3: Job 1 [11]

Figure 2.4: Job 2 [11]

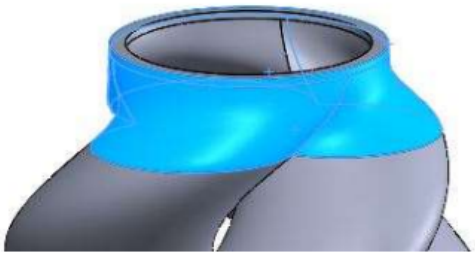

Figure 2.5: Spiral junction

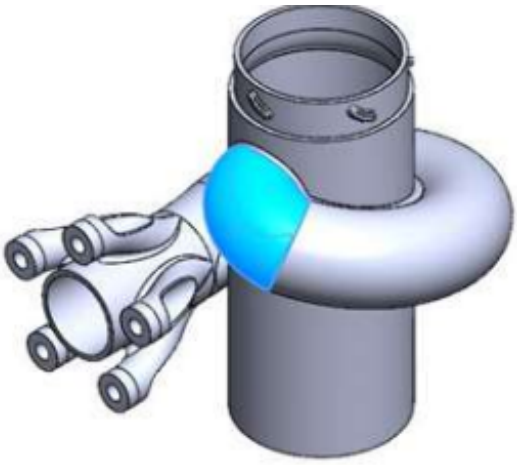

Figure 2.6: Perpendicular junction

Figure 2.5 and Figure 2.6 will then be the respective starting references for the

geometries studied in this thesis that from now on will be referred to as Manufact 1 and Manufact 2.

2.2 Manufact 1

2.2.1 The problem

As described in [11] the spiral is realized by slicing the tubes with planes perpendicular to their trajectories and then rotating of 120° to align with the next tube so that the deposition head is always tangent to the tube surface avoiding overhangs. The geometry must also avoid collision with the head so some parameters are adjusted to achieve it. The problem is that once the junction must be created, the tubes converge and collide with the path of the head. Furtherly to that, mantaining the head tangent to the tubes would require a too high of an hoverhang.

Traditional process

Traditional processes are sometimes used for complex tubular geometries, and one example is the realization of Automotive exhaust pipes. Some of these processes are:

- Bending
- Welding of small sections
- Machining

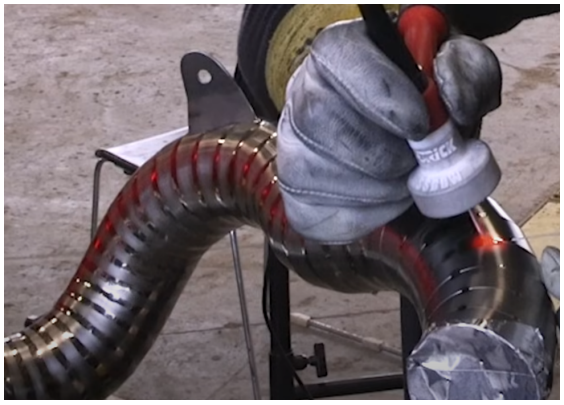

Figure 2.7: Custom Automotive Exhaust

The problem is that processes like the one in Figure 2.7 are not only time consuming and labor expensive, but often limited for complex geometries like Figure 2.2. Thats why DED-LB might be a solution.

2.2.2 The suggestion

Realizing the Junction of the spiral (Figure 2.5) as it is it's not feasible, therefore the model needs some adjustments. Since the approach described in [11] is already proven to be successful, only the geometry of the junction itself will be studied. Since the maximum overhang achievable without too noticeable defects is demonstrated to be 10° on the vertical (Figure 2.8) the first tentative will be to remodel the junction in order to achieve a geometry that presents overhangs not larger than the feasible ones.

Figure 2.8: Overhang effects from 5° to 25°

This solution should allow the junction to be printed with a planar slicing with planes all perpendicular to the axis of the spiral. The only issue is that in this way, the minimum height of the complete transition to a single tube would be constrained by trigonometrical relationships and is demonstrated to be of **131 mm** from the section of the first contact btetween the three circumferences that form the tubes.

Anyway for the moment we decided to only test the geometry until the three tubes are fully merged, which corresponds to an height of the sample of **17 mm**. The spiral was modelled by asuming a 180° turn in an height of 200mm, therefore a pitch of 400mm, and a each tube with a radius of 22mmm every 120° degrees. Since the thickness had to be 2mm just as the width of the deposition, only the mid surface was swept along the helix, imposing the path to be normal on the first and last sections. This should help the feasibility since in this way the we can force the maximum taper of the junction to stay within the operative range of the machine, but first of all the limit overhang must be investigated.

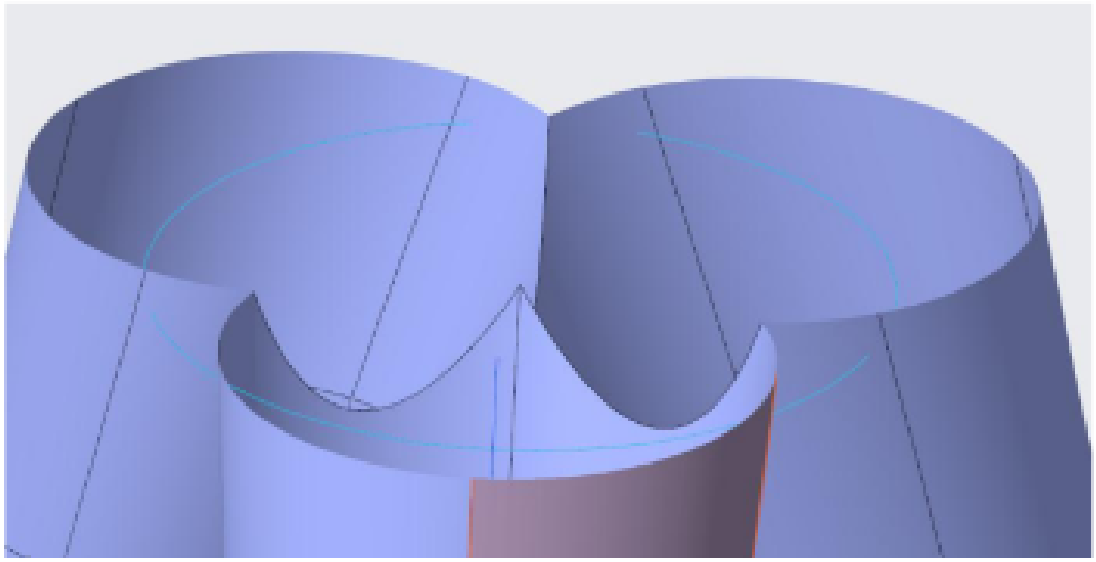

Figure 2.9: Giunction of the spiral

2.3 Manufact 2

The Problem

Even if in [11] a 90°-bend cruve is realized by an inovative slicing logic, it still doesn't address the issue with the joining section with a perpendicular tube. T-section tubes are widely spread in modern engineering, but the DED-LB technology presents some issue that make their realization a challenge.

2.3.1 Traditional process

T-Shape tubes are traditionally obtained by cutting pre-exsiting tubes and then welding them togheter. Another, but more complex approach, is hydroforming (Figure 2.10).

The main challenge of printing the T-shape tube is that two curvatures develop on different planes at the same time in the area where the two tubes merge, and the machine has a maximum effective overhang of 10°. This means we are almost forced to realize that the tube maintaining the head is perpendicular to the tube's axis. The first step is to identify which tube we are talking about. For this reason, from now on we will refer to the tube that "hosts" the other (That has a hole in it) as **Tube A** and the other as **Tube B**.

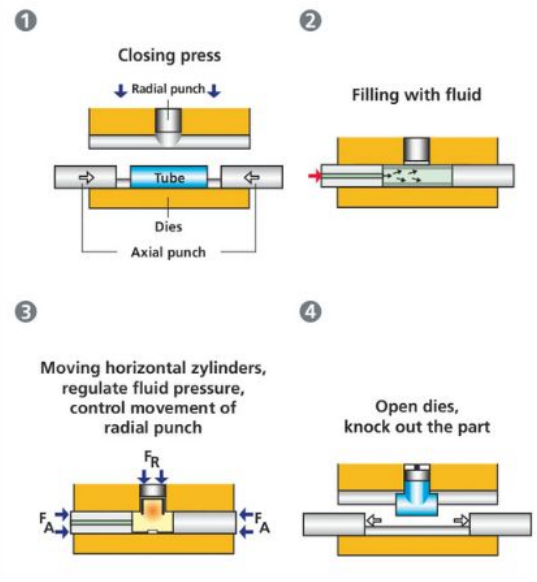

H

Figure 2.10: Hydroforming process for T-Shape Tubes

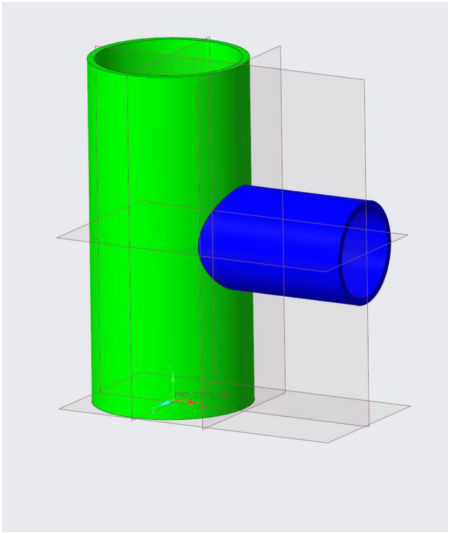

Figure 2.11: Tube A in green - Tube B in blue

2.3.2 The suggestion

Since the Tube A has two curvatures that develop in the layers concerning the intersection hole, we must avoid at least one. For this reason the intersection geometry is modified by creating a diamond-shape hole as in figure 2.13.

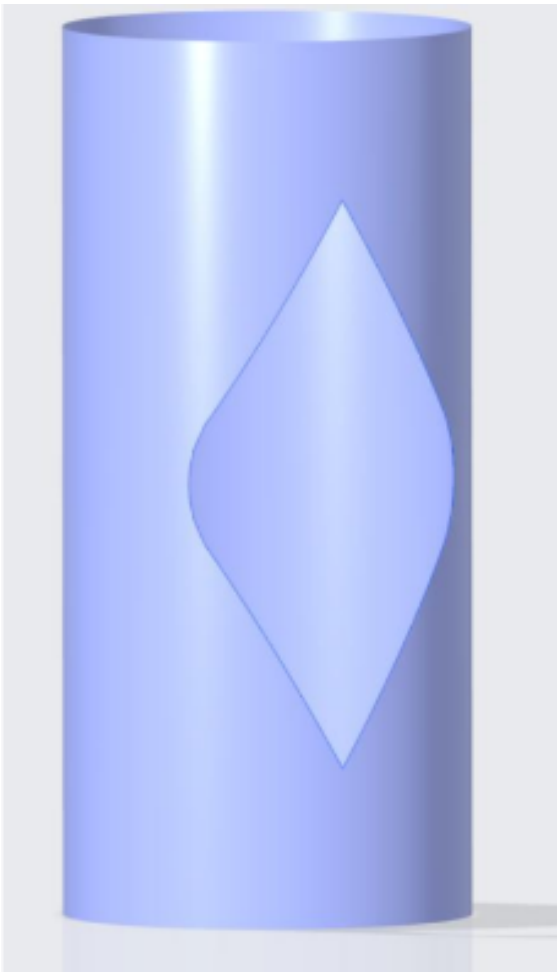

Figure 2.12: Tube A hole

The shape of the hole is realized in two sections of constant tilt:

- **The first section** by creating the circular hole until an angle of 10° with respect to the horizontal direction, then joining this point with the point found by intersecting the tangent to the original circular hole with a tilt of 10° to the one with a tilt of 20°. The same shall be done with the tangent of 30°.

- **The second section** is achieved by connecting the last point with the intersection point between the vertical symmetry axis and the last tangent found.

The hole is realized follwing the algorithm in B.
Therefore the Tube B section can be lofted to join the Tube A as in 2.13

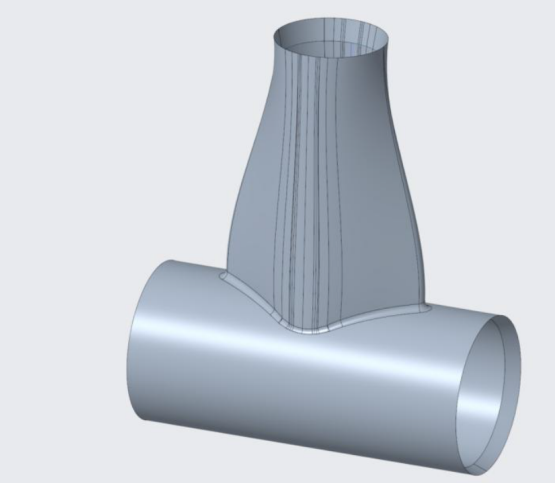

Figure 2.13: Tube A in green - Tube B in blu

Chapter 3

Test Geometries

3.0.1 Test Geometry 1

Test 1

At this point was clear that the main obstacle is the maximum overhang angle that the machine can tolerate. Before attempting to print the complete tube, it was essential to evaluate the deposition strategy using a simplified mock geometry. As illustrated, this geometry consists of a flat wall with extremities tilted at angles of +10° and -10° relative to the vertical Z-axis.
The chosen deposition strategy involves slicing the wall geometry, as detailed in Appendix A, to determine the necessary coordinates for generating the G-code. The deposition head is programmed to align tangentially with the tilted edges at the wall's extremities. Upon completion of each lateral section, the head returns to a position normal to the local X'Y' plane to deposit the central segment while maintaining the deposition bed angle. Subsequently, the head gradually tilts again to become tangential to the opposite edge.
Dividing the wall into distinct sections aims to maximize the duration during which the head deposits material with the bed's normal parallel to the global XY plane. This approach simplifies the G-code generation process.
The number of points defining each layer's lateral portions is significantly higher than those defining the central portion. This increased density is necessary due to the system's rotation around the global X-axis, which does not intersect the origin of the local reference frame O', as explained in 1.2.2. Consequently, each incremental rotation step requires recalculating the corresponding global coordinates, necessitating distinct transformation matrices for each point.
To simplify calculations, global coordinates of locally defined points are initially obtained by applying a rotation around the local Z-axis (**Z'**) followed by a rotation around the global X-axis (**X**). Thus, the rotation matrices are determined directly

from the inputs A and B specified for the deposition machine:

$$R_{z'}(A) = \begin{bmatrix} \cos A & -\sin A & 0 \\ \sin A & \cos A & 0 \\ 0 & 0 & 1 \end{bmatrix} \tag{3.1}$$

$$R_x(B) = \begin{bmatrix} 1 & 0 & 0 \\ 0 & \cos B & -\sin B \\ 0 & \sin B & \cos B \end{bmatrix} \tag{3.2}$$

And based on the initial offset vector $\Delta Z = [0,0,85]$, we can find the total equation:

$$\mathbf{p}\text{glob} = R_x(\theta_x) \cdot [Rz'(\theta_z) \cdot \mathbf{p}_{\text{loc}} + \Delta Z] \tag{3.3}$$

The code that is used to extract the final matrix of the global points that are each time transformed is present in Appendix C.2

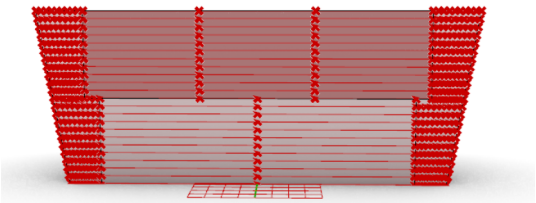

Figure 3.1: Test geometry 1 slicing

Figure 3.2: Deposition test of test geometry 1

Despite this logical approach, the experimental results were inconclusive. The dense clustering of points where the tilt of the deposition bed returned to zero, along with the finite size of the laser spot, caused the deposition head to repeatedly rotate at the same point. This resulted in material accumulation and noticeable defects in the deposited layers, even when different movement feed rates were tested.

Test 2

In the second set of tests, a simpler method was applied by defining only three points per layer: two points positioned on the tilted sides and one central point. Rather than applying complex transformation matrices, only translation matrices were used. Additionally, the **G72/73 - Part Surface Coordinates [PSC]** command was implemented.
Initially, the G-code was structured to have the deposition head start tangent to

one side, move across to the opposite side by briefly eliminating the tilt at the central point, and then return to tangency. The use of PSC guaranteed consistent velocity throughout the deposition trajectory. Additionally, a retraction routine was integrated, causing the deposition head to first retract along the Z-axis, allowing the deposition plate to return to its default position. Before starting each new layer, the system moved to the updated coordinates and re-tilted the deposition bed accordingly.

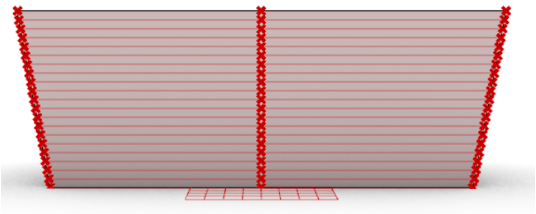

Figure 3.3: Test geometry 1 slicing

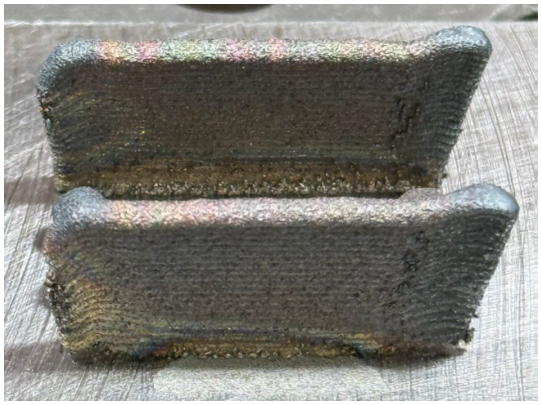

Figure 3.4: Deposition test of test geometry 1

Since it is easy to notice the difference between the starting and arriving edge (the starting edge is the right edge in Figure 3.4) we tried to compensate for this effect by implementing a layer alternation routine as in Appendix **??**.

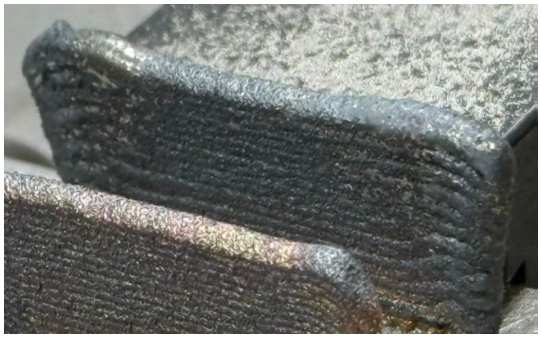

Figure 3.5: Alternate layers

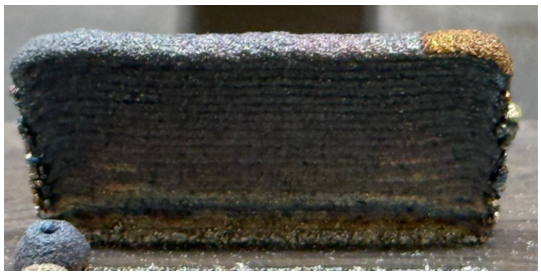

Figure 3.6: Alternate layers with pause

Alternating the layers appears to be the optimal strategy. However, the previous approach allowed about 7 seconds per layer, which provided sufficient cooling time for the deposition area before the laser was applied again. With alternating layers, the first point of the new layer coincides exactly with the last point of the previous one. Even though the laser briefly switches off between layers, residual heat remains at the spot. This residual heat can inadvertently cause sintering of the powder, as the powder flow cannot be halted immediately due to system inertia. To address this issue, we introduced a 3-second pause between layers, as shown in Figure 3.6. Since the maximum overhang that develops in the actual manufact is 30°, we performed a test on the geometry modifying the tilt of the edges to this value but keeping the the logic and KPIs unaltered from the last test.

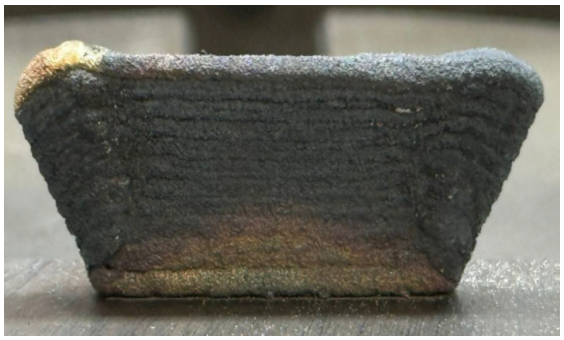

Figure 3.7: Test Geometry with 30° overhang

3.0.2 Test Geometry 2

As easily deductable from the manufact geometries, the overhangs that are present are actually holes, so the next step is to achieve the junction of two overhangs. Therefore another mock geometry was tested as in figure 3.8.

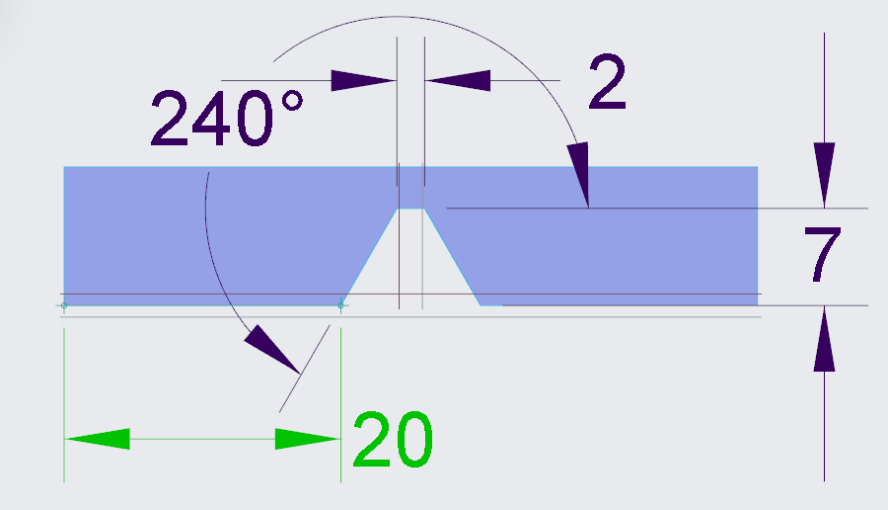

Figure 3.8: Test Geometry with hole *(quotes in mm)*

The hole was modeled to maintain the overhanging edge with a tilt of 30°, but the junction segment was forced to an eight of 7mm and to be 2mm wide. The last quote is due to the fact that the slicing algorithm is capable of extracting only the corner, so only half of the laser would be "inside" the hole. A total of 13 tests were performed varying different process parameters such as Powder feeding rate, Laser Power and Movement speed.

(a) Test 1

(b) Test 2

(c) Test 3

(d) Test 4

(e) Test 5

(f) Test 6

(g) Test 7

(h) Test 8

(i) Test 9

(j) Test 10

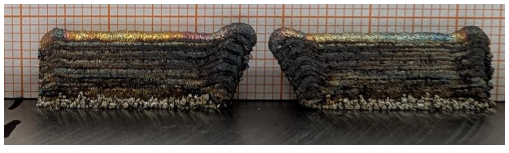

(k) Test 11

(l) Test 12

Figure 3.9: Experimental test geometries arranged in two columns and six rows.

To better understand the approach, we must look at Figure 3.10. In fact the code itself present in Appendix E works upon the definition of these 4 points. In particular with forcing the deposition head to be tangent to the overhanging edges on points 2 and 4 and by depositing each layer in two phases, one for each segment. All the depositions were performed without the last layers above the junction.

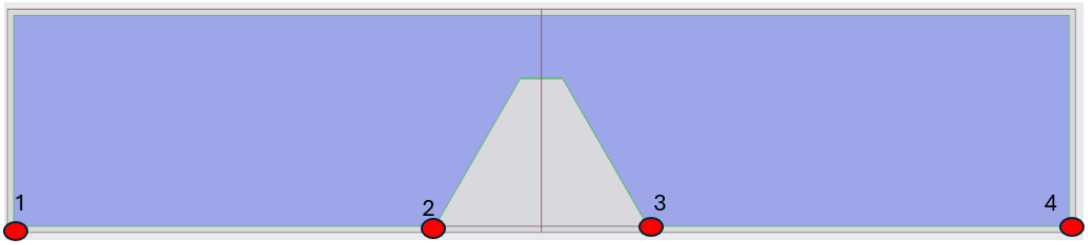

Figure 3.10: Four points identification

The first three tests (Figures 3.9a, 3.9b, 3.9c) were carried out by depositing in order segment 1-2 and then, after retraction and e reset of the table segment 4-3. The movement of the head was therefore "inward" for each layer. From test 4 to test 10, the deposition was performed with an "outward" movement for each segment. The last two tests were performed by alternating the layers. The precise set of parameters adopted are reported in the Table 3.1.

Measurements

Table 3.1: Measured heights for each deposition test. The column *Rp* indicates the rotation speed of the powder feeder.

Test	Strategy	Power [W]	Feed rate [mm/min]	Rp [rpm]	H1 [mm]	H2 [mm]	H3 [mm]	H4 [mm]	ΔH [mm]
1	–	550	700	–	10.66	11.44	11.18	10.71	2.45
2	External–internal	550	–	–	10.52	11.22	10.65	10.86	2.61
3	External–internal	500	–	–	9.39	10.55	9.63	9.35	2.80
4	Internal–external	550	–	–	9.38	9.99	9.32	10.04	0.56
5	Internal–external	400	–	–	8.86	9.62	8.73	9.57	0.24
6	Internal–external	400	950	9	8.96	9.64	8.88	9.56	0.03
7	Internal–external	400	1050	7.5	8.58	9.53	8.59	9.29	0.49
8	Internal–external	500	950	9	10.09	10.40	10.29	10.84	2.75
9	Internal–external	500	950	9	8.83	9.56	8.90	9.24	2.60
10	Internal–external	500	950	9	8.47	9.27	8.50	9.00	0.53
11	Alternated	550	1050	9	9.21	9.54	9.16	9.34	0.39
12	Alternated	400	950	7.5	8.39	9.28	8.41	9.89	1.44

The height measurements collected from the twelve deposition trials provide valuable insight into the influence of process parameters and deposition strategy on the tested geometry. Given that each layer has a nominal thickness of 0.5 mm, the

complete wall corresponds to approximately 20 layers (10 mm total height). For the first nine tests, the upper layers were intentionally removed, so the nominal height around the hole should be about 7 mm. The last three tests, instead, include all layers and thus target a final height of approximately 10 mm.

3.0.3 Successful junction

By implementing the lessons learned in the previous section, the last test was conducted on the geometry but with all the layers gave good results as the junction is finally joined in a successful way.

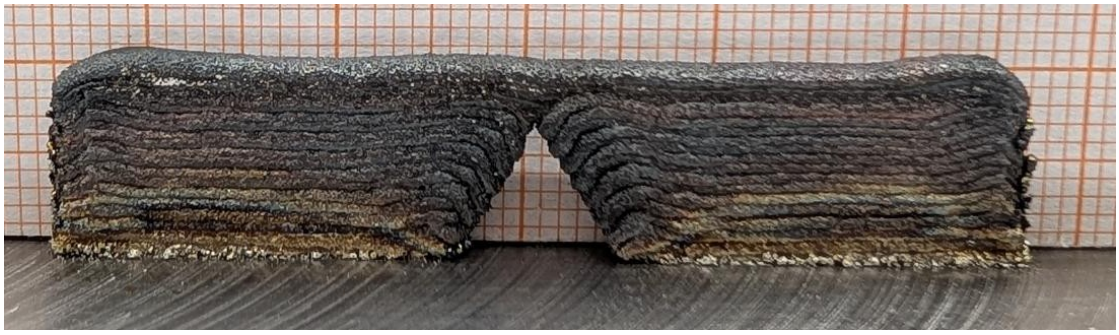

Figure 3.11: Junction completed succesfully

This means that the final geometry of the Manufact 2 can be realized if the approach described in this chapter can be successfully applied to a circular trajectory, thus simplifying the geometry of the hole as in Figure 3.12 as it becomes a projection of the hole from the wall to the cylindrical surface of the tube.

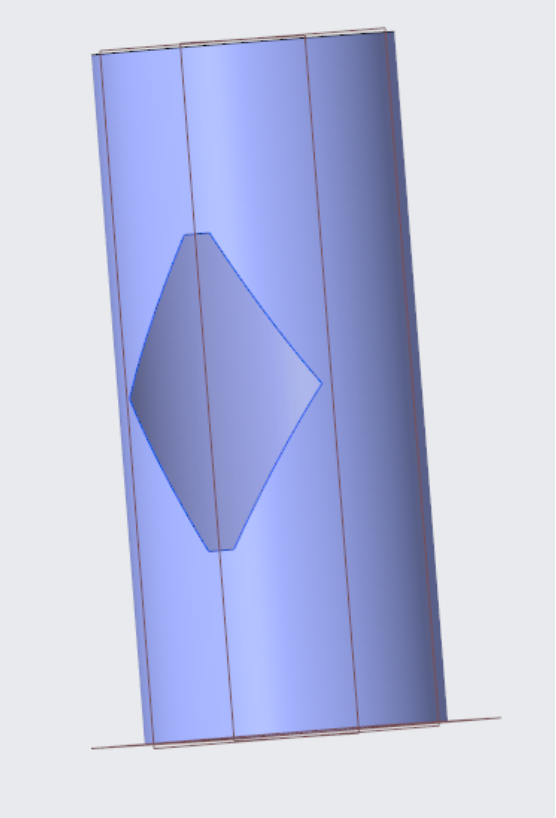

Figure 3.12: New design of Manufact 2

Overall trends

A general overbuild is observed in almost all samples without the upper layers (Tests 1–9): measured heights range between 8.5 mm and 11.5 mm, i.e., up to 3–4 mm higher than the intended 7 mm. This means that, although the deposition stopped before the final layers, the effective layer thickness or the local material accumulation exceeded the nominal 0.5 mm per layer. Such behavior is typical of conditions characterized by a **high specific energy input**—mainly due to high laser power (500–550 W), high powder feed rotation (Rp), and low scanning speed [4],[8]. The excess energy causes a deeper and wider melt pool, which increases the deposition rate and results in a thicker bead, leading to loss of dimensional accuracy and overbuild.
Conversely, the last three tests (Tests 10–12), in which all layers were deposited, reached total heights slightly below the nominal 10 mm. This indicates a moderate underbuild, likely due to the combination of higher scanning speed and lower powder efficiency in the upper layers, where thermal accumulation is less significant.

Influence of the deposition strategy

The choice of the scanning strategy — *external-to-internal*, *internal-to-external*, or *alternating* — strongly affects the resulting geometry.

- **External-to-internal (Tests 1–3).** These samples show the largest deviations ($\Delta H \approx 2.4$–2.8 mm) and the most pronounced *edge swelling* near the hole boundaries (points H2 and H4). High laser power ($\geq$500 W) combined with high Rp promotes a deeper and wider melt pool [13], leading to excessive material accumulation at the edges. The molten material tends to flow toward the hole opening, increasing the local height and partially closing the nominal gap.

- **Internal-to-external (Tests 4–9).** This configuration provides much better uniformity ($\Delta H \leq 0.5$ mm for most cases). The head moves away from the hole region during deposition, preventing thermal accumulation and stabilizing the melt pool. The optimal balance was achieved with 400 W, a scanning speed of 950–1050 mm/min, and Rp between 7.5 and 9 rpm, resulting in nearly constant heights across the four measurement points (e.g., Test 6: $\Delta H = 0.03$ mm). However, the absolute height still exceeds the 7 mm target, indicating a uniform but energetically rich process that produces thicker layers overall.

- **Alternating direction (Tests 11–12).** Alternating the deposition direction between layers improved the symmetry of thermal distribution and reduced the asymmetry between the left and right sides of the wall. The overall height remained slightly below 10 mm, while uniformity was acceptable ($\Delta H = 0.4$–1.4 mm). This strategy appears effective in reducing cumulative distortion but not necessarily in correcting height errors.

Effect of process parameters

The results confirm the strong coupling between **laser power**, **scanning speed**, and **powder feed rotation (Rp)**. Similar relationships are well-documented in literature for laser-based Directed Energy Deposition (DED) processes, where the specific energy input per unit length defines the melt pool morphology and, consequently, the dimensional accuracy of the part [4, 8].

- **Laser power.** Increasing the laser power from 400 W to 550 W amplifies the melt pool volume and the deposition rate, leading to overbuild and loss of geometric control. A higher energy input per unit area results in deeper melting and excessive layer thickness [8, 13].

- **Scanning speed.** Increasing the scanning speed (from 950 to 1050 mm/min) reduces the specific energy input and therefore limits the melt pool depth and the layer height, resulting in improved geometric stability and reduced overbuild [4].
- **Powder feed rotation (Rp).** The Rp value directly controls the mass flow rate of powder into the melt pool. Higher Rp (around 9 rpm) correlates with thicker deposited layers and, when combined with low scanning speed, causes material accumulation and surface swelling. Conversely, a lower Rp (7.5 rpm) produces thinner and more stable layers, particularly when coupled with moderate laser power (400 W) [14].

Gap and local non-uniformities

The variation among H1–H4 points (ΔH) quantifies the geometric gap between different regions of the layer. Large ΔH values (>2 mm) are associated with high Rp and high power (P $\geq$ 500 W), where the edges (H2, H4) become significantly higher than the central zones due to molten material flowing toward the hole. With the internal-to-external strategy and moderate Rp, ΔH drops below 0.5 mm, confirming a more balanced thermal regime and uniform solidification. A small ΔH, however, does not guarantee dimensional accuracy: even uniform layers may accumulate excessive thickness if the powder flow and energy input per unit length are not properly tuned.

Correlation with literature

The observed trends are consistent with previously published studies on laser-directed energy deposition. Gibson et al. [4] and Wang et al. [8] demonstrated that excessive energy density—resulting from high laser power or low scanning speed—produces wider and deeper melt pools, leading to overbuilding and geometric distortion. Similarly, Godec et al. [14] reported that an increased powder feed rate enhances the material deposition rate but, when the energy input is not properly adjusted, results in thicker layers and reduced dimensional accuracy. Lu et al. [13] experimentally confirmed that the melt pool depth and bead width are directly correlated with laser power and inversely correlated with scanning speed. The present experimental results, showing overbuild for high power and Rp, and improved stability at moderate parameter combinations, are therefore fully aligned with these process–structure relationships.

Chapter 4

Conclusions

The experimental campaign, although partially inconclusive in terms of dimensional accuracy, provided several important lessons both on the process parameters of deposition and on the geometric preparation of the model. These findings guided the refinement of the G-code generation strategy, the optimization of the slicing procedure, and the adjustment of the process parameters for improved reproducibility and geometric fidelity.

Process-related conlcusions

From the analysis of the deposition tests, it was observed that the final height and uniformity of the wall are primarily governed by the combination of laser power, scanning speed, and powder feed rotation (Rp). Excessive energy input—resulting from high laser power and high Rp at low scanning speed—produces a larger and deeper melt pool, leading to thicker layers and pronounced overbuild [4, 8]. Conversely, moderate power (around 400 W), scanning speeds between 950 and 1050 mm/min, and Rp between 7.5 and 9 rpm ensure more stable deposition, improved layer uniformity, and reduced geometric distortion [14, 13].

Among the scanning strategies tested, the *internal-to-external* configuration proved the most effective in limiting thermal accumulation near the hole and achieving uniform heights ($\Delta H \leq 0.5$ mm). The *external-to-internal* path, on the other hand, generated higher edge swelling and partial closure of the hole due to the flow of molten material toward the center. The *alternating* strategy successfully balanced thermal asymmetries between layers but did not fully correct height deviations.

In summary, the tests highlighted that overbuild is primarily driven by excessive energy input and powder feed rate, while uniformity depends on maintaining a consistent and moderate specific energy input per unit length. The most stable configuration was achieved at 400 W, 950–1050 mm/min, and Rp between 7.5 and

9 rpm. To reach the nominal 7 mm height in the hole region, a slight reduction of both laser power (350–380 W) and Rp (6–7 rpm) is recommended, possibly combined with a power ramp-down at the end of each segment. For the complete 10 mm walls, one or two finishing layers at lower energy and powder feed should be added to close the top surface without introducing overbuild.

Model and toolpath-related lessons

Three major lessons were learnt regarding model preparation, slicing, and G-code generation.

Lesson 1 — G-code structure. The sequence of commands must follow a strict order to ensure proper synchronization between laser and movement. The first point must be reached in G5 mode (Exact Position) for maximum accuracy; the G72 (PSC) must be active before any movement is started, so that the table rotation is compensated; the M60 (Laser ON) command must be placed **before** the G7 interpolation, otherwise the movement begins before laser activation; and the M61 (Laser OFF) must be inserted after a G5 command to avoid premature deactivation of the laser during motion.

Listing 4.1: Example of generated G-code for one deposition layer

```
;___LAYER 1___   2-1/3-4   []   1-2/4-3
G5 G1 X-5.041 Y0.000 Z91.500 A0.00 B30.00 F950 ; MOVE TO START NEW
    LAYER
G72
M60 ; LASER ON
G7
X-25.041 Y0.000 A0.00 B0.00
G5
M61 ; LASER OFF
;--END OF FIRST SEGMENT--

;--RETRACTION--
Z101.50 ; RAISE THE HEAD
G4 X0.0

;--PREPARE NEXT SEGMENT--
A0.00 B-30.00
X5.041 Y0.000 ; ALIGN NEW POINT
Z91.50 ; DROP TO NEW POINT
G72

;--START SECOND SEGMENT--
M60 ; LASER ON
G7
```

```
X25.041 Y0.000 Z91.50 A0.00 B0.00 ; Fourth point
G5
M61 ; LASER OFF

;--RETRACTION--
Z101.50
G4 X0.0

;--END OF LAYER 1--
```

Lesson 2 — Slicing accuracy. The Grasshopper slicing method, which relies on mathematical intersections between slicing lines and the 3D surface, can sometimes fail to detect points located exactly at the inclined edges of the hole. To correct this, the CAD geometry was slightly modified by increasing the hole height from 7.00 mm to 7.04 mm. This minimal adjustment forces the algorithm to capture the missing corner points without affecting the actual printed geometry, as the variation is well below the machine's spatial resolution. Figure 4.1 shows the missing corner points before correction, while Figure 4.2 illustrates the corrected geometry.

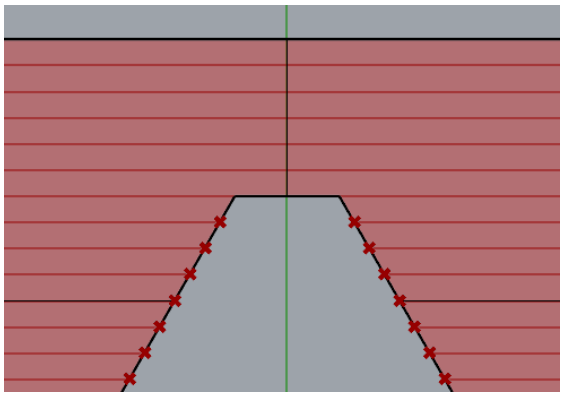

Figure 4.1: Missing points on the inclined edges of the hole.

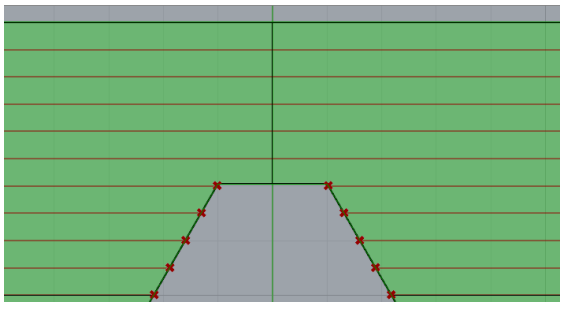

Figure 4.2: Corrected geometry with the corner points included.

Lesson 3 — Laser footprint and geometric interference. The finite size of the laser beam introduces local shadowing effects near the junction of the hole. When the head is directed toward the last point of the second segment of the penultimate layer, part of the laser beam is obstructed by the previously deposited material, resulting in an estimated interference of approximately 0.13 mm. To eliminate this interference, the geometry was adjusted by extending the joining segment length to 2.23 mm, ensuring full laser accessibility. As shown in Figure 4.3, this correction significantly improved deposition quality. The use of alternating layers (Tests 11 and 12) further mitigated this issue by distributing the thermal input symmetrically.

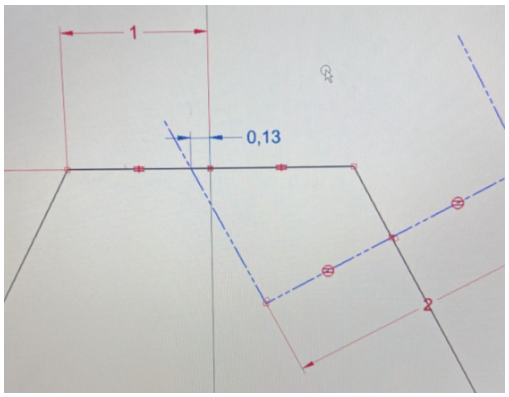

(a) Original geometry with laser interference.

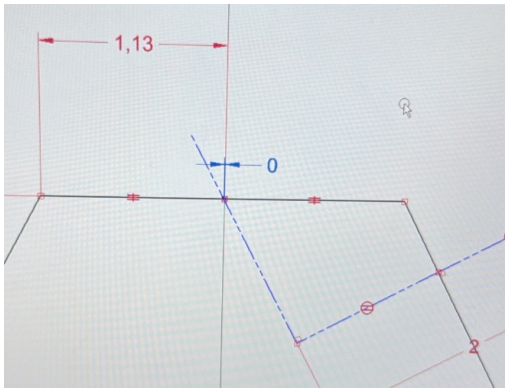

(b) Modified geometry with corrected clearance.

Figure 4.3: Comparison between the two geometries for the hole region.

Chapter 5

Considerations

Overall, the combination of experimental observations and model refinements provided a deeper understanding of the DED-LB process. The results confirmed that both the control of process parameters and the precision of geometric modeling play an essential role in achieving dimensional accuracy. The lessons learnt from these tests have therefore been incorporated into the subsequent development of optimized G-code generation and adaptive deposition strategies, aimed at minimizing overbuild, maintaining uniform layer thickness, and ensuring consistent deposition across complex geometries.

Further developments can be envisioned building upon the work presented in this thesis. One of the most significant next steps could be the realization of Tube B of Manufact 2 (Figure 2.11). This geometry could be created by lofting the circular cross-section of the tube with the inner contour of the hole, thus generating a smooth, continuous transition between the two shapes. The manufacturing approach would follow the same concept adopted for Tube A: the deposition head should remain tangent to the surface throughout the process by tilting the deposition plate, effectively minimizing the overhang relative to the Z-axis and ensuring a consistent layer buildup.

Moreover, the MATLAB scripts developed for this work provide a strong foundation for future automation. They could be refined and integrated into a dedicated toolbox to streamline and accelerate the G-code generation process, since they already include well-structured routines and a robust logical framework for producing complex geometries with adaptive control of deposition parameters.

Appendix A

Slicing with Grasshopper

Once the 3D model is ready, it is imported as an .igs on Rhinoceros. Then by means of the extension *Grasshopper* the model is sliced with planes parallel to the X'Y' plane on the local reference system of the geometry. The logic is to slice separatedly the portions that needs the head to be tilted and the portions that need no tilt. Since the tilt of the head varies linearly from the first to the last point of the portion of the layer, we cannot just use the first and last point transformed in the global reference system, as the rotation will be implemented linearly and movement will not result in the desired geometry. For this reason, the number of points is increased to 10 so that the MatLab code can rotate at each step and better approximate the geometry.

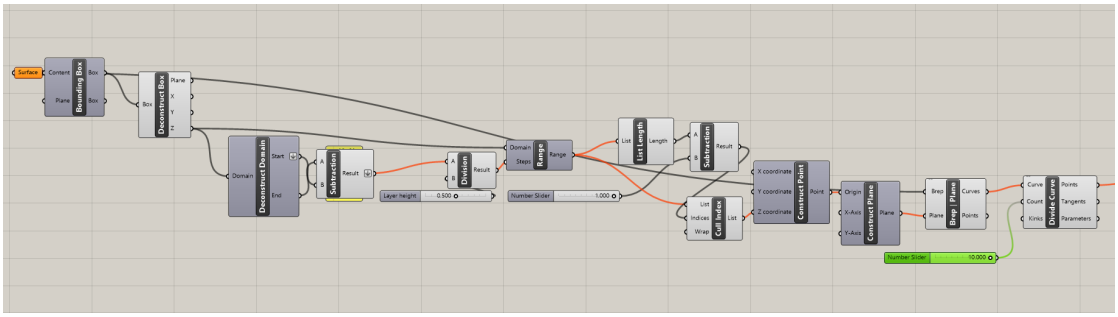

Figure A.1: Enter Caption

Here is reported the workflow from Grasshopper

1. Import the geometry

   Load your geometry (surface or solid) into Grasshopper from Rhino. You can import directly from the Rhino model or from external files such as IGES, STL, or STEP, using the appropriate import components or plugins.

2. Compute the bounding box

   Calculate the bounding box of your geometry. This gives you the overall dimensions and helps you determine the minimum and maximum Z-values for the slicing process.

3. Set layer thickness and generate Z-values

   Use a Number Slider to set your desired layer thickness. Then, generate a list of Z-values (the heights at which you will slice) using a Range or Series component. These Z-values define the spacing and number of slicing planes.

4. Create slicing planes

   Create a series of XY planes at the calculated Z-heights. Use a Plane component and set its origin to each Z-value from your list, so each plane is parallel to the XY plane and at the correct height.

5. Intersect planes with geometry

   Use the Brep | Plane intersection component. For each slicing plane, this will intersect it with the geometry and return one or more intersection curves, which represent the contours at each layer.

6. Discretize intersection curves

   Use the Divide Curve component to split each intersection curve into a series of points. These points can then be used as waypoints for your toolpath (e.g., for additive manufacturing or CNC).

7. (Optional) Calculate tangents, normals, or angles

   If your process requires 5-axis machining or more complex movement, you can use the Evaluate Curve component to get tangents, normals, or angles at each toolpath point.

8. Remove the last layer (if needed)

   To avoid slicing above the object, remove the last slicing plane. You can do this by getting the list length (number of planes), subtracting 1 with an Expression (x-1), and using Cull Index to remove the last plane from your list.

Appendix B

T-tube hole coordinates

Given the chance to exploit overhang angles up to 10°, the hole can be constructed in steps rotating the axis of Tube A of 10° with respect to the Z-Axis for each step. This means that the top half of Tube A will be realized in different sections of constant tilt, and as shown in Figure B.1 each section of constant tilt will have to be finished by filling a cuspidal hole on the side opposite to the hole. Since this hole is filled by realigning the Tube A axis with the Z-Axis, its taper must allow the head to be positioned. This means that we cannot accept a number of steps greater than the ratio:

$$\frac{Head\ Taper}{Max\ Overhang} = 3\ steps$$

So the hole will be generated in three steps, and to make sure that it is as small as possible will be generated according to the following logic applied only to te top right quarter circumference that identifies the original hole:

1. Find the lines tangent to the original circular hole at each angular step. The coordinates of the points of the tangents will be:

$$\begin{aligned} A_i &= (x_i, y_i) \\ &= (R\cos(i\theta),\ R\sin(i\theta)) \end{aligned}$$

   The equations of the tangent lines will be given by:

$$\begin{aligned} y - y_i &= m_i(x - x_i) \\ m_i &= -\cot(i\theta) = \frac{-\sin(i\theta)}{\cos(i\theta)} \end{aligned}$$

2. Find the intersection point (P_i) between two consecutive tangents t_i and t_{i+1}.

$$
\begin{aligned}
x &= \frac{m_i x_i - m_{i+1} x_{i+1} + y_{i+1} - y_i}{m_i - m_{i+1}} \\
y &= m_i(x - x_i) + y_i \\
P_i &= (x, y)
\end{aligned}
$$

3. Find the point of intersection of the tangents with the vertical symmetry axis of Tube A.
   This helps to show that using the maximum number of steps grants also the minimum "height" of the hole (which in this case is 32 mm from the centre).

$$
\begin{aligned}
y &= -m_i x_i + y_i \\
O_i &= \Big(0,\ -m_i x_i + y_i\Big)
\end{aligned}
$$

4. Trace an arc of 10° of the original hole and connect A_1 with P_1, P_1 with P_2 and P_2 with O_3.

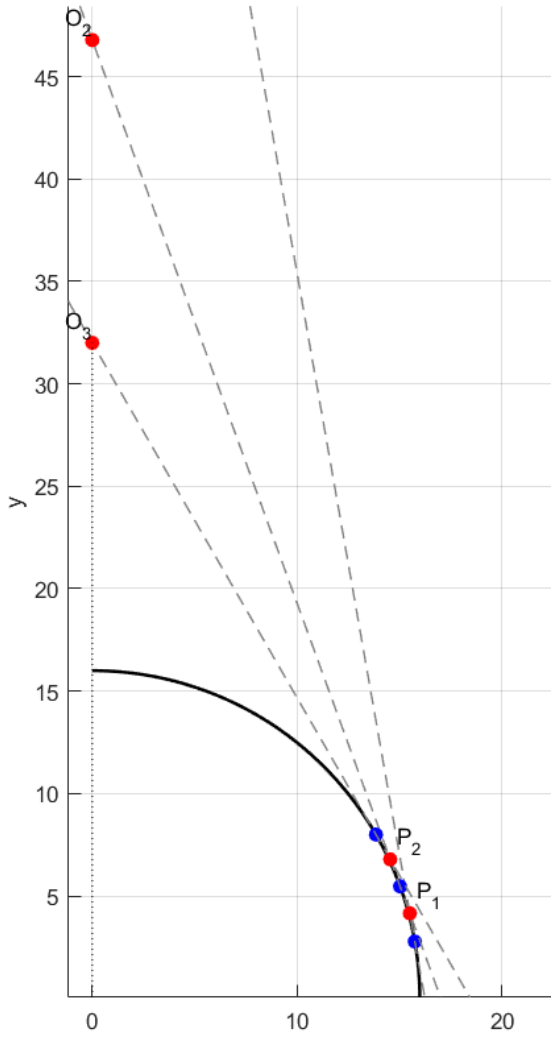

Figure B.1: Points for the Hole

Listing B.1: Script for the points of the hole profile

```
% Parametri
R = 16;
theta_deg = 10;
theta = deg2rad(theta_deg); % in radianti

n_p = 2;                % numero di punti P_i
n_tg = n_p + 1;         % numero di tangenti necessarie
n = n_tg;

% Punti della circonferenza per disegno
```

```
t = linspace(0, pi/2, 200);
x_circ = R * cos(t);
y_circ = R * sin(t);

figure; hold on; axis equal; grid on;
plot(x_circ, y_circ, 'k', 'LineWidth', 1.5); % circonferenza nera

% Inizializza array
points = zeros(n, 2);
slopes = zeros(n, 1);
O = zeros(n, 2);      % coordinate O_i (intersezione con asse Y)
P = zeros(n-1, 2);    % coordinate P_i (intersezione tra tangenti)

for i = 1:n
    angle = i * theta;  % Evita angle = 0
    x = R * cos(angle);
    y = R * sin(angle);
    points(i, :) = [x, y];

    % Punto blu sulla circonferenza
    plot(x, y, 'bo', 'MarkerSize', 6, 'MarkerFaceColor', 'b');

    % Coefficiente angolare della tangente (usa cos/sin per stabilità)
    m = -cos(angle) / sin(angle);
    slopes(i) = m;

    % Tangente (tratto sottile grigio)
    x_vals = linspace(x - R, x + R, 200);
    y_vals = m * (x_vals - x) + y;
    plot(x_vals, y_vals, '--', 'Color', [0.5 0.5 0.5], 'LineWidth', 0.8);

    % Intersezione con asse Y (x = 0)
    xO = 0;
    yO = m * (xO - x) + y;
    O(i, :) = [xO, yO];
    plot(xO, yO, 'ro', 'MarkerSize', 6, 'MarkerFaceColor', 'r');
    text(xO, yO, sprintf(' O_{%d}', i), 'VerticalAlignment', 'bottom', 'HorizontalAlignment', 'right');
end

% Calcolo dei punti di intersezione tra tangenti (P_i)
for i = 1:n-1
    x0 = points(i, 1); y0 = points(i, 2); m0 = slopes(i);
    x1 = points(i+1, 1); y1 = points(i+1, 2); m1 = slopes(i+1);

    X = (m0*x0 - m1*x1 + y1 - y0) / (m0 - m1);
    Y = m0 * (X - x0) + y0;
```

```
57
58      P(i, :) = [X, Y];
59      plot(X, Y, 'ro', 'MarkerSize', 6, 'MarkerFaceColor', 'r');
60      text(X, Y, sprintf(' P_{%d}', i), 'VerticalAlignment', 'bottom',
        'HorizontalAlignment', 'left');
61  end
62
63  % Assi centrati rispetto alla circonferenza
64  xlim([-R, 2.5*R]);
65  ylim([-0.5*R, 2*R]);
66  plot(0, 0, 'k+'); % centro della circonferenza
67
68  % Assi cartesiani
69  line([-R, 2.5*R], [0, 0], 'Color', 'k', 'LineStyle', ':');
70  line([0, 0], [-0.5*R, 2*R], 'Color', 'k', 'LineStyle', ':');
71
72  title('Tangenti, Intersezioni P_i, e Proiezioni O_i (Coordinate
        salvate)');
73  xlabel('x'); ylabel('y');
```

Appendix C

Code for Transformation Matrixes

C.1 Local Points Extractor

The first section of the code reads the .txt file in which all the coordinates of the points defined in the local reference system are saved and organizes them by layer and with an incremental order of absolute position (from left to right).

Listing C.1: Local Points Extractor

```
1
2 clear; clc;
3
4 % ---- Percorso file punti ----
5 filename_points = INSERT DIRECTORY OF POINTS.TXT;
6
7 % ---- Lettura punti dal file ----
8 fid = fopen(filename_points);
9 str = textscan(fid, '%s', 'Delimiter', '\n');
10 str = str{1};
11 fclose(fid);
12
13 N = numel(str);
14 data = zeros(N,3);
15 for i = 1:N
16     s = strrep(str{i}, '{', '');
17     s = strrep(s, '}', '');
18     vals = sscanf(s, '%f, %f, %f');
19     data(i,:) = vals';
20 end
21
```

```
% ---- Ordina prima per Z crescente, poi per Y crescente (da sx a dx per ogni layer) ----
data = sortrows(data, [3 2]); % 3: z (layer), 2: y (da sx a dx)

% ---- Raggruppa per layer (z) con tolleranza e elimina doppioni ----
tol = 1e-6;
z_list = data(:,3);

z_unique = [];
for i = 1:length(z_list)
    if isempty(z_unique) || all(abs(z_unique - z_list(i)) > tol)
        z_unique = [z_unique; z_list(i)];
    end
end

Nlayers = length(z_unique);
LayerData = cell(Nlayers,1);

for i = 1:Nlayers
    idx = abs(data(:,3) - z_unique(i)) < tol;
    pts = data(idx,:);
    [~, ia, ~] = unique(pts, 'rows', 'stable'); % Elimina eventuali doppioni
    pts = pts(ia, :);
    LayerData{i} = pts;
end

% ---- Salva la cella LayerData su file ----
save('LayerData.mat', 'LayerData');
clear all
clc
```

C.2 Transformation algorithm

This section transforms all the points with the relative transformation matrix relative to the tilt asset of the head of each point

Listing C.2: Trasnformation algorithm

```
clear all; clc
run LayerData_Extractor_2000.mlx
load('LayerData.mat');

for k = 1:size(LayerData,1)
    Points_local = LayerData{k};      % punti [n x 3]
    n_points = size(Points_local,1);
    offset = [0; 0; 80];

    steps_curve_1 = 10;
    A_start_1 = 10;  A_end_1 = 0;
    A_steps_1 = linspace(A_start_1, A_end_1, steps_curve_1);
    B_start_1 = 0;   B_end_1 = 0;
    B_steps_1 = linspace(B_start_1, B_end_1, steps_curve_1);

    steps_curve_2 = 10;
    A_start_2 = 0    ;  A_end_2 = -10;
    A_steps_2 = linspace(A_start_2, A_end_2, steps_curve_2);
    B_start_2 = 0;   B_end_2 = 0;
    B_steps_2 = linspace(B_start_2, B_end_2, steps_curve_2);

    % Indici per la parte finale
    new_indexes = (n_points - steps_curve_2 + 1) : n_points;

    % Inizializza matrice risultati
    Points_glob = zeros(n_points, 5);

    % Primo tratto: A da 10   a 0
    for i = 1:steps_curve_1
        theta_x = deg2rad(A_steps_1(i));   % X globale (in radianti)
        theta_z = deg2rad(B_steps_1(i));   % Z' locale (in radianti)
        Rz = [cos(theta_z) -sin(theta_z) 0;
              sin(theta_z)  cos(theta_z) 0;
              0          0          1];
        Rx = [1 0 0;
              0 cos(theta_x) -sin(theta_x);
              0 sin(theta_x)  cos(theta_x)];
        p_loc = Points_local(i,:)';          % colonna 3x1
        p_tmp = Rz * p_loc + offset;
        p_glob = Rx * p_tmp;
```

```
41          Points_glob(i,:) = [p_glob', rad2deg(theta_z), rad2deg(
    theta_x)];
42      end
43
44      % Tratto finale: A da 0   a -10
45      for i = 1:steps_curve_2
46          idx = new_indexes(i);
47          theta_x = deg2rad(A_steps_2(i));   % X globale (in radianti)
48          theta_z = deg2rad(B_steps_2(i));   % Z' locale (in radianti)
49          Rz = [cos(theta_z) -sin(theta_z) 0;
50                sin(theta_z)  cos(theta_z) 0;
51                0          0          1];
52          Rx = [1 0 0;
53                0 cos(theta_x) -sin(theta_x);
54                0 sin(theta_x)  cos(theta_x)];
55          p_loc = Points_local(idx,:)';        % colonna 3x1
56          p_tmp = Rz * p_loc + offset;
57          p_glob = Rx * p_tmp;
58          Points_glob(idx,:) = [p_glob', rad2deg(theta_z), rad2deg(
    theta_x)];
59      end
60
61      % Tratto centrale: nessuna rotazione, solo traslazione
62      if steps_curve_1 + 1 < new_indexes(1)
63          for i = steps_curve_1 + 1 : new_indexes(1) - 1
64              p_loc = Points_local(i,:)';      % colonna 3x1
65              p_glob = p_loc + offset;         % nessuna rotazione
66              Points_glob(i,:) = [p_glob', 0, 0];
67          end
68      end
69
70      % Salva risultati per questo layer
71      Points_Ready{k} = Points_glob;
72  end
73
74  Points.global= Points_Ready'; % (opzionale, se vuoi colonna di celle)
75  Points.local= LayerData;
76
77  save("Points.mat", "Points")
78  clear all;clc;
79  load Points.mat
```

Appendix D

MATLAB script for point extraction and layer organization of Test Geometry 2

The following MATLAB script (`LayerDataExtractor.m`) processes the planar section points exported from the CAD model. It groups the data by layer (based on the Z coordinate), orders the points along the boundary, corrects their orientation, and adds rotation parameters (A, B) for the subsequent G-code generation.

Script description

- **Initialization:** definition of file path, head rotation parameter B_{default}, vertical offset Z_{offset}, and tolerances for Z quantization and duplicate removal.
- **File reading:** imports the coordinate file `Punti.txt` as a matrix (X, Y, Z) using flexible delimiters.
- **Layer grouping:** quantizes Z within a tolerance to merge points belonging to the same deposition layer.
- **Point sorting:** points within each layer are ordered along the contour using a convex hull algorithm; if it fails, sorting is done by polar angle.
- **Orientation check:** ensures clockwise ordering for consistent deposition direction.

- **Angle columns:** adds $A = 0$ for all points and alternates $B = \pm B_{\text{default}}$ for four-point layers.
- **Offset and saving:** adds Z_{offset} to all layers and saves the final data structure `LayerData.mat`.

MATLAB Code

```
clear all
clc

%% == Initial Parameters ==
filePath = "C:\Users\paolo\Desktop\PoliTo\TESI\TEST SETTEMBRE\
    Ricominciamo\Parete\Punti.txt";
B_default = 30;         % B on 2nd and 4th point in 4-point layers
Z_offset  = 91.5;       % Offset added to all Z
tolZ      = 1e-3;       % tolerance for grouping Z layers
tolDup    = 1e-9;       % tolerance for removing duplicate XY(Z)

%% == File Reading ==
fid = fopen(filePath, 'r');
if fid == -1
    error('File not found: %s', filePath);
end
C = textscan(fid, '%f%f%f', 'Delimiter', '{} ,\t', ...
    'MultipleDelimsAsOne', true, 'CollectOutput', true);
fclose(fid);
data = C{1};  % Nx3 matrix [X Y Z]

%% == Layer Grouping with Tolerance ==
Z = data(:,3);
Zq = round(Z./tolZ)*tolZ;              % quantized Z to avoid split
uniqueZ = unique(Zq, 'stable');
nLayers = numel(uniqueZ);
LayerData = cell(nLayers,1);

%% == Build LayerData ==
for k = 1:nLayers
    % 1) Select points belonging to current layer
    idx = (Zq == uniqueZ(k));
    pts = data(idx, :);

    % 2) Remove duplicates with tolerance
    pts = uniquetol(pts, tolDup, 'ByRows', true);

```

```
    % 3) Sort points along contour (convex hull)
    X = pts(:,1); Y = pts(:,2);
    if size(pts,1) >= 3
        try
            K = convhull(X, Y);
            ordIdx = K(1:end-1);
        catch
            % fallback: sort by angle if convex hull fails
            xc = mean(X); yc = mean(Y);
            ang = atan2(Y - yc, X - xc);
            [~, ordIdx] = sort(ang, 'descend'); % clockwise
        end
    else
        ordIdx = 1:numel(X);
    end

    sortedPts = pts(ordIdx, :);

    % 4) Force clockwise order
    s = sum(sortedPts(:,1).*circshift(sortedPts(:,2),-1) ...
          - sortedPts(:,2).*circshift(sortedPts(:,1),-1));
    if s > 0
        sortedPts = flipud(sortedPts);
    end

    % 5) Add A=0 and B (only for 4-point layers)
    N = size(sortedPts, 1);
    Acol = zeros(N, 1);
    Bcol = zeros(N, 1);
    if N == 4
        Bcol(2) =  B_default;
        Bcol(3) = -B_default;
    end

    % 6) Apply Z offset
    sortedPts(:,3) = sortedPts(:,3) + Z_offset;

    % 7) Save layer [X Y Z A B]
    LayerData{k} = [sortedPts, Acol, Bcol];
end

save LayerData.mat
```

The generated `LayerData.mat` file contains a cell array where each element represents one deposition layer with columns:

$$[X,\ Y,\ Z,\ A,\ B]$$

This data structure is later used to automatically produce the G-code for the DED-LB system.

Appendix E

G-code Compiler for Test Geometry 2

This appendix presents the final MATLAB script used to generate the G-code for the wall geometry with alternating toolpath directions and variable head angles. The code processes the structured data from `LayerData.mat`, defines deposition parameters, and automatically compiles the final CNC file.

Listing E.1: MATLAB G-code Compiler for Variable-Angle Wall

```
clear all; clc;

%% === USER-DEFINED PARAMETERS ===
% === OUTPUT FILE NAME AND DIRECTORY ===
gcode_name = 'Parete_alternati_01.cnc';
gcode_dir  = 'C:\Users\paolo\Desktop\PoliTo\TESI\TEST SETTEMBRE\Ricominciamo\Parete\Angoli variabli';

% Create destination folder if it does not exist
if ~exist(gcode_dir, 'dir')
    mkdir(gcode_dir);
end

% Full path to the G-code file
gcode_filename = fullfile(gcode_dir, gcode_name);

% === PROCESS PARAMETERS ===
feedrate_lavorazione = 950;      % [mm/min] - Deposition feedrate
feedrate_retrazione  = 950;      % [mm/min] - Retraction feedrate
```

```
Z_retract             = 10.0;     % [mm]      - Retraction height
PAUSA_END_LAYER       = 0;        % [s]       - Dwell time at layer end (G4 X...)
alterna_layer         = true;     % Alternate direction between layers (true/false)
laser_power           = 550;      % [W]       - Laser power

% === LOAD LAYER DATA ===
load("LayerData.mat");

% Open output file for writing
fid = fopen(gcode_filename, 'w');
if fid == -1
    error('Cannot open file %s for writing!', gcode_filename);
end

%% === PRINT START ROUTINE ===
fprintf(fid, '; ===== START OF BUILD ROUTINE =====\n');
fprintf(fid, 'G00 G17 G71 G90\n');
fprintf(fid, 'G99\n');
fprintf(fid, 'G76\n');
fprintf(fid, 'G17 G90\n');
fprintf(fid, 'G00 A0. B0.\n');
fprintf(fid, 'G72\n');
fprintf(fid, '$POWDER_FEED(ON, 9., OFF, 0)\n');
fprintf(fid, 'M302 PR.2\n');
fprintf(fid, 'G04 X10.\n');
fprintf(fid, 'M50 P%.1f\n', laser_power);
fprintf(fid, 'M100\n');

%% === MAIN LOOP: LAYER GENERATION ===
for k = 1:numel(LayerData)

    % --- Case 1: Layers with 4 points ---
    if size(LayerData{k},1) == 4
        if alterna_layer == 1
            if mod(k,2) == 1
                % Odd layers     normal order
                P = LayerData{k};
                x2=P(1,1); y2=P(1,2); z2=P(1,3); a2=P(1,4); b2=P(1,5);
                x1=P(2,1); y1=P(2,2); z1=P(2,3); a1=P(2,4); b1=P(2,5);
```

```
58                  x4=P(4,1); y4=P(4,2); z4=P(4,3); a4=P(4,4);
    b4=P(4,5);
59                  x3=P(3,1); y3=P(3,2); z3=P(3,3); a3=P(3,4);
    b3=P(3,5);
60              else
61                  % Even layers     reversed order
62                  P = LayerData{k};
63                  x1=P(1,1); y1=P(1,2); z1=P(1,3); a1=P(1,4);
    b1=P(1,5);
64                  x2=P(2,1); y2=P(2,2); z2=P(2,3); a2=P(2,4);
    b2=P(2,5);
65                  x3=P(4,1); y3=P(4,2); z3=P(4,3); a3=P(4,4);
    b3=P(4,5);
66                  x4=P(3,1); y4=P(3,2); z4=P(3,3); a4=P(3,4);
    b4=P(3,5);
67              end
68          else
69              % No alternation     same path every layer
70              P = LayerData{k};
71              x2=P(1,1); y2=P(1,2); z2=P(1,3); a2=P(1,4); b2=P
    (1,5);
72              x1=P(2,1); y1=P(2,2); z1=P(2,3); a1=P(2,4); b1=P
    (2,5);
73              x4=P(4,1); y4=P(4,2); z4=P(4,3); a4=P(4,4); b4=P
    (4,5);
74              x3=P(3,1); y3=P(3,2); z3=P(3,3); a3=P(3,4); b3=P
    (3,5);
75          end
76
77          % --- Layer header ---
78          fprintf(fid, '; --- LAYER %d ---\n', k);
79          fprintf(fid, 'G5 G1  X%.3f Y%.3f Z%.3f A%.2f B%.2f F
    %.0f ; Move to start point\n', ...
80                  x1,y1,z1,a1,b1,feedrate_lavorazione);
81
82          % --- Segment 1 (point 1     2) ---
83          fprintf(fid, 'G72\n');
84          fprintf(fid, 'M60 ; LASER ON\n');
85          fprintf(fid, 'G7\n');
86          fprintf(fid, 'X%.3f Y%.3f A%.2f B%.2f\n', x2,y2,a2,
    b2);
87          fprintf(fid, 'G5\n');
88          fprintf(fid, 'M61 ; LASER OFF\n');
89          fprintf(fid, '; End of first segment\n\n');
90
```

```
91          % --- Retraction before next path ---
92          fprintf(fid, '; Retraction\n');
93          fprintf(fid, 'Z%.2f ; Raise head\n', z1 + Z_retract)
    ;
94          fprintf(fid, 'G4 X%.1f\n\n', PAUSA_END_LAYER);
95
96          % --- Move to next segment (point 3) ---
97          fprintf(fid, '; Prepare next segment\n');
98          fprintf(fid, 'A%.2f B%.2f\n', a3, b3);
99          fprintf(fid, 'X%.3f Y%.3f ; Move to point 3\n', x3,
    y3);
100         fprintf(fid, 'Z%.2f ; Drop to layer height\n', z3);
101         fprintf(fid, 'G72\n\n');
102
103         % --- Segment 2 (point 3     4) ---
104         fprintf(fid, '; Start second segment\n');
105         fprintf(fid, 'M60 ; LASER ON\n');
106         fprintf(fid, 'G7\n');
107         fprintf(fid, 'X%.3f Y%.3f Z%.2f A%.2f B%.2f ; Move
    to point 4\n', ...
108                 x4,y4,z4,a4,b4);
109         fprintf(fid, 'G5\n');
110         fprintf(fid, 'M61 ; LASER OFF\n');
111         fprintf(fid, 'Z%.2f ; Retract\n', z4 + Z_retract);
112         fprintf(fid, 'G4 X%.1f\n', PAUSA_END_LAYER);
113         fprintf(fid, '; --- End of layer %d ---\n\n', k);
114
115     % --- Case 2: Layers with 2 points ---
116     else
117         P = LayerData{k};
118         if alterna_layer && mod(k,2)==0
119             % Reverse order on even layers
120             x1=P(2,1); y1=P(2,2); z1=P(2,3); a1=P(2,4); b1=P
    (2,5);
121             x3=P(1,1); y3=P(1,2); z3=P(1,3); a3=P(1,4); b3=P
    (1,5);
122         else
123             x1=P(1,1); y1=P(1,2); z1=P(1,3); a1=P(1,4); b1=P
    (1,5);
124             x3=P(2,1); y3=P(2,2); z3=P(2,3); a3=P(2,4); b3=P
    (2,5);
125         end
126
127         % --- Single-segment layer ---
128         fprintf(fid, '; --- LAYER %d ---\n', k);
```

```
129         fprintf(fid, 'G72\n');
130         fprintf(fid, 'G5 X%.3f Y%.3f Z%.2f A0 B0 F%.0f\n',
    x1, y1, z1, feedrate_lavorazione);
131         fprintf(fid, 'M60 ; LASER ON\n');
132         fprintf(fid, 'G7\n');
133         fprintf(fid, 'X%.3f Y%.3f Z%.2f\n', x3, y3, z3);
134         fprintf(fid, 'M61 ; LASER OFF\n\n');
135     end
136 end
137
138 %% === END-OF-JOB ROUTINE ===
139 fprintf(fid, '; ===== END OF JOB =====\n');
140 fprintf(fid, 'G5\n');
141 fprintf(fid, 'M61 ; LASER OFF\n');
142 fprintf(fid, 'G00 Z%.3f\n', 150);
143 fprintf(fid, 'M50 P0\n');
144 fprintf(fid, 'M101\n');
145 fprintf(fid, '$POWDER_FEED(OFF, 0, OFF, 0)\n');
146 fprintf(fid, 'B0. A0.\n');
147 fprintf(fid, 'M02\n');
148
149 % Close file
150 fclose(fid);
151 disp(['G-code successfully saved in ', gcode_filename])
```

The script automatically generates the complete CNC file for deposition, including start-up routines, layer-by-layer motion control, and final shutdown sequence. Layer alternation, retraction height, and laser parameters can be modified in the user-defined section at the beginning of the code.

1. User-defined parameters

In the first part, the user defines the file name, the output directory, and the process parameters. The code automatically checks whether the specified folder exists and creates it if necessary. Among the editable parameters, the most relevant are:

- **`feedrate_lavorazione`**: deposition feed rate [mm/min];
- **`feedrate_retrazione`**: feed rate used for retraction moves [mm/min];
- **`Z_retract`**: height increment for vertical retraction between segments [mm];
- **`PAUSA_END_LAYER`**: pause duration (G4 dwell) at the end of each layer [s];
- **`alterna_layer`**: logical flag to alternate toolpath direction between successive layers (`true`/`false`);

- `laser_power`: laser power used during deposition [W].

The `LayerData.mat` file is then loaded: it contains all points grouped by layer, with the corresponding coordinates and head angles A and B. Each layer is stored as a matrix with five columns [X, Y, Z, A, B].

—

2. Initialization of the G-code file

The script opens a new output file and writes the initial setup routine of the CNC program. This part includes:

- setting the active coordinate plane and units (`G17, G71, G90`);
- enabling the powder feed and laser system;
- defining the laser power (`M50 P...`) and a short pre-heating pause (`G04 X10.`);
- homing of rotational axes A and B to zero.

This section ensures that the deposition process starts in a controlled state, with the correct setup of the machine and beam parameters.

—

3. Main loop: layer generation

The core of the code consists of a loop over all layers contained in `LayerData`. Each iteration generates the full G-code instructions for one layer, based on the number of points (either two or four).

- **Layers with four points:** These correspond to closed rectangular sections. The algorithm alternates the point order depending on the parity of the layer index (k), effectively alternating the deposition direction between odd and even layers. This strategy minimizes heat accumulation and improves structural symmetry.

  For each layer:

  1. the head moves to the starting point at working height;
  2. the laser is activated (`M60`) and the first segment is deposited (points 1–2);
  3. the laser is turned off (`M61`), and a retraction is performed along the Z-axis;
  4. the head repositions to the next segment (points 3–4);

5. the laser is turned on again, and the second segment is deposited;
6. a final retraction and optional pause are executed before moving to the next layer.

- **Layers with two points:** These correspond to open or linear sections. The logic is simplified: only one deposition pass is performed per layer, again with the option to alternate direction across layers.

The layer numbering and progress are also logged in the G-code file using semicolon-prefixed comments (`; -- LAYER n --`) for readability.

—

4. End-of-job routine

Once all layers are processed, the script writes the shutdown commands for the deposition system:

- deactivation of the laser and powder flow (`M61, $POWDER_FEED(OFF,...)`);
- head retraction to a safe Z height (150 mm);
- power-down of the laser (`M50 P0`) and termination of the job with `M02`.

This final section ensures the safe conclusion of the build process and returns the machine to a neutral state.

—

Summary

Overall, the program automates the entire toolpath compilation process for multi-layer L-DED builds, integrating:

- alternation of deposition directions;
- control of laser and motion synchronization;
- automatic retraction and repositioning between segments;
- final shutdown procedures.

This modular structure allows straightforward modification of process parameters, making the script adaptable to other geometries or experimental setups.

Bibliography

[1] ISO/ASTM International. *Additive Manufacturing — General principles — Fundamentals and vocabulary*. International Standard. Geneva, Switzerland: International Organization for Standardization, 2021. URL: https://www.iso.org/standard/82921.html (cit. on pp. 1–3).

[2] R. Bashir, M. Ahmed, A. Khan, et al. «Additive Manufacturing Processes and Applications: A Comprehensive Review». In: *Materials* 17.5 (2024), p. 1856. DOI: 10.3390/ma17051856 (cit. on p. 3).

[3] E. Atzeni and A. Salmi. *Costs and Cost Effectiveness of Additive Manufacturing*. Tech. rep. NIST SP 1176. National Institute of Standards and Technology (NIST), 2014. DOI: 10.6028/NIST.SP.1176 (cit. on p. 3).

[4] Ian Gibson, David Rosen, and Brent Stucker. *Additive Manufacturing Technologies: 3D Printing, Rapid Prototyping, and Direct Digital Manufacturing*. 3rd. New York, USA: Springer, 2021. DOI: 10.1007/978-3-031-17449-0 (cit. on pp. 3, 32–35).

[5] A. Gomez, D. Rossi, and G. Falcone. «Smart Materials for Additive Manufacturing: Trends and Perspectives». In: *Sensors* 24.9 (2024), p. 2668. DOI: 10.3390/s24092668 (cit. on p. 3).

[6] S. Kumar, C. Lee, and X. Zhang. «Additive Manufacturing in Aerospace Industry: Applications and Challenges». In: *Metals* 9.12 (2019), p. 1286. DOI: 10.3390/met9121286 (cit. on p. 3).

[7] F. de Souza, J. Martins, T. Silva, and R. Costa. «Additive Manufacturing in the Automotive Sector: A Review of Challenges and Opportunities». In: *Applied Sciences* 13.4 (2023), p. 2312. DOI: 10.3390/app13042312 (cit. on p. 3).

[8] S. Wang, J. Li, and X. Chen. «Advances and Challenges in Additive Manufacturing for Metal Components». In: *Journal of Manufacturing Processes* (2023) (cit. on pp. 3, 32–35).

[9] Gabriele Piscopo, Eleonora Atzeni, Abdollah Saboori, and Alessandro Salmi. «An Overview of the Process Mechanisms in the Laser Powder Directed Energy Deposition». In: *Applied Sciences* 13.1 (2023). ISSN: 2076-3417. DOI: 10.3390/app13010117. URL: https://www.mdpi.com/2076-3417/13/1/117 (cit. on pp. 7, 8).

[10] «430BD Maintenance Manual (rev.E)». In: () (cit. on pp. 12, 13).

[11] Santo Polizzi. «Design e realizzazione di un artefatto di riferimento per la tecnologia di deposizione diretta di metallo». Tesi di Laurea Magistrale in Ingegneria Meccanica. Torino, Italy: Politecnico di Torino, 2025 (cit. on pp. 14, 16–20).

[12] Federico Mazzucato, Alberta Aversa, Roberto Doglione, Sara Biamino, Anna Valente, and Mariangela Lombardi. «Influence of Process Parameters and Deposition Strategy on Laser Metal Deposition of 316L Powder». In: *Metals* 9 (Oct. 2019), p. 1160. DOI: 10.3390/met9111160 (cit. on pp. 14, 15).

[13] Q. Lu, S. Li, Y. Zhang, and J. Xu. «Experimental Study on the Influence of Process Parameters on Melt Pool Geometry in Laser-Directed Energy Deposition». In: *Additive Manufacturing* 35 (2020), p. 101244 (cit. on pp. 33–35).

[14] Damir Godec et al. «Introduction to Additive Manufacturing». In: *A Guide to Additive Manufacturing*. Ed. by Damir Godec, Joamin Gonzalez-Gutierrez, Axel Nordin, Eujin Pei, and Julia Ureña Alcázar. Cham: Springer International Publishing, 2022, pp. 1–44. ISBN: 978-3-031-05863-9. DOI: 10.1007/978-3-031-05863-9_1. URL: https://doi.org/10.1007/978-3-031-05863-9_1 (cit. on pp. 34, 35).